ANNALS OF PHYSICS 132, 237–276 (1981)

A Simple Method for Evaluating Goldstone Diagrams in an Angular Momentum Coupled Representation*

T. T. S. KUO,† J. SHURPIN, AND K. C. TAM

Department of Physics, State University of New York at Stony Brook, Stony Brook, New York 11794

E. OSNES

Institute of Physics, University of Oslo, Oslo 3, Norway

AND

P. J. ELLIS‡

School of Physics and Astronomy, University of Minnesota, Minneapolis, Minnesota 55455

Received May 20, 1980

A simple and convenient method is derived for evaluating linked Goldstone diagrams in an angular momentum coupled representation. Our method is general, and can be used to evaluate any effective interaction and/or effective operator diagrams for both closed-shell nuclei (vacuum to vacuum linked diagrams) and open-shell nuclei (valence linked diagrams). The techniques of decomposing diagrams into ladder diagrams, cutting open internal lines and cutting off one-body insertions are introduced. These enable us to determine angular momentum factors associated with diagrams in the coupled representation directly, without the need for carrying out complicated angular momentum algebra. A summary of diagram rules is given.

1. INTRODUCTION

One of the fundamental problems in nuclear structure physics is to calculate the properties of finite nuclei starting from the free nucleon–nucleon interaction. Since only a few low-lying states are generally of physical interest, the first step is to formulate

* Work supported in part by DOE Contracts EY-76-S-02-3001 and AT(11-1)-1764 and by Norwegian Research Council of Science and Humanities.

† Nordita Guest Professor at University of Oslo (Fall Semester, 1978), Alexander von Humboldt Foundation Awardee at Institut für Kernphysik, Kernforschungsanlage Jülich (Spring Semester, 1979).

‡ On quarter leave at State University of New York at Stony Brook (Spring Semester, 1978).

0003-4916/81/040237–40$05.00/0

the problem in terms of an effective interaction acting in a strongly truncated Hilbert space (a model space with a finite number of states).

To be more specific, consider the nuclear structure problem of ^{18}O—the prototype nucleus for effective interactions—which has two neutrons more than the closed-shell nucleus ^{16}O. Instead of considering the true 18-particle eigenvalue problem

$$H\Psi_n = E_n\Psi_n , \tag{1}$$

which of course cannot be solved exactly, we study the more tractable and probably more meaningful model problem consisting of two nucleons in the $1s0d$ shell outside an ^{16}O closed-shell core. Then, inside this model space we have to use an effective Hamiltonian H_{eff} to account for the neglected degrees of freedom. Thus, the ^{18}O model space eigenvalue problem can be written as

$$PH_{\text{eff}}P\Psi_m = (E_m - E_0^c)\, P\Psi_m , \qquad m = 1, 2,..., d. \tag{2}$$

Here, P is a projection operator

$$P = \sum_{i=1}^{d} |\, \Phi_i\rangle\langle\Phi_i \,|, \tag{3}$$

projecting onto the model space spanned by unperturbed shell-model states Φ_i consisting of an inert ^{16}O core and two valence nucleons in the $1s0d$ shell. Further, in Eq. (2) E_0^c is the ^{16}O ground state energy. We may consider Eq. (2) as the defining equation for H_{eff}. Thus, H_{eff} is defined to reproduce exactly the binding energies of d states in ^{18}O relative to the binding energy of the ^{16}O ground state. The corresponding wave functions are then projections of the exact wave functions Ψ_m onto the model space.

For ^{18}O, and any other nucleus with two valence nucleons, the effective Hamiltonian can be divided into a one-body and a two-body part

$$\begin{aligned} H_{\text{eff}} &= H_{\text{eff}}^{(1)} + H_{\text{eff}}^{(2)} , \\ H_{\text{eff}}^{(1)} &= \sum_i \tilde{\epsilon}_i a_i^\dagger a_i , \\ H_{\text{eff}}^{(2)} &= \tfrac{1}{4} \sum_{ijkl} \langle ij \mid V_{\text{eff}} \mid kl\rangle\, a_i^\dagger a_j^\dagger a_l a_k . \end{aligned} \tag{4}$$

The operator $a_i^\dagger$ (a_i) creates (annihilates) a single fermion in the state i. These operators appear in diagrams as the external lines. In studies of ^{18}O, it is customary not to calculate $H_{\text{eff}}^{(1)}$. Rather, the $\tilde{\epsilon}_i$ are taken as the experimental energies of the lowest $J^\pi = 5/2^+$, $1/2^+$, and $3/2^+$ states in ^{17}O. Hence, our main effort is directed toward the calculation of $H_{\text{eff}}^{(2)}$. Nevertheless, in so doing we also need to evaluate one-body diagrams because they contribute to $H_{\text{eff}}^{(2)}$ by way of the folded diagrams which are part of V_{eff} (see below). However, our technique is quite general and is readily applied

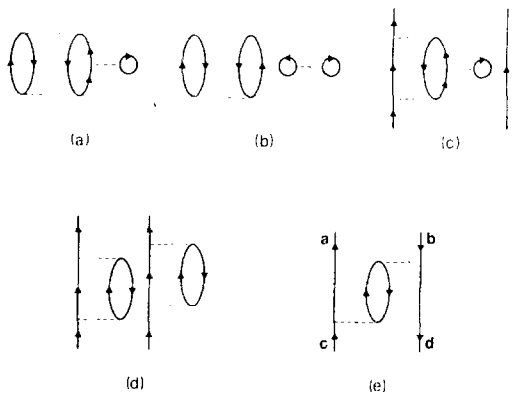

FIG. 1. Some linked and unlinked diagrams. Interaction vertices are represented by dashed lines.

to nuclei with more than two valence nucleons (i.e., Eq. (4) for H_{eff} contains terms up to $H_{\text{eff}}^{(n)}$ for n valence nucleons), as outlined in Subsection 3.7, below.

The effective interaction can be expressed as a perturbation series in the free nucleon–nucleon interaction, using either a time-dependent perturbation theory [1, 2] or a time-independent perturbation theory [3, 4]. This is formally exact, but, of course, actual calculations can only be approximate, given the many-body nature of the problem. Modern many-body perturbation theories are often expressed in a diagrammatic language. These methods have several advantages over the old-fashioned, purely algebraic methods. Firstly, many terms which cancel among each other are eliminated from the outset. Secondly, one has a systematic way of enumerating the various contributions, and is less likely to miss out terms. Thirdly, diagrams illustrate in a rather direct way the physical processes involved, allowing one to use physical intuition in selecting the important terms. Last, but not least, diagrams are spectacular and beautiful, and are even fun to work with.

As is well known, for the ground state of a closed-shell nucleus the energy shift (from the unperturbed energy) is given by the sum of all linked vacuum to vacuum diagrams. In Fig. 1, diagram (a) is of such a form, but not (b). For nuclei with valence particles, a convenient way to generate the effective interaction diagrams is the so-called Q-box formulation [2, 5, 6]. In this language the effective interaction can be written schematically as[1]

$$V_{\text{eff}} = \hat{Q} - \hat{Q}' \int \hat{Q} + \hat{Q}' \int \hat{Q} \int \hat{Q} - \hat{Q}' \int \hat{Q} \int \hat{Q} \int \hat{Q} + \cdots. \tag{5}$$

Here, $\hat{Q}$ (generally termed $\hat{Q}$-box) is an infinite sum of diagrams, typical members of which are diagrams (c), (d) and (e) in Fig. 1. They are valence linked and irreducible in the sense that all interactions must be linked to at least one valence line and all intermediate states must contain at least one passive line (i.e., a non-valence line, see,

[1] Here, it is understood that the purely one-body component of H_{eff} is removed, as described in Ref. [5].

for example, Ref. [1]). The $\hat{Q}$-box formulation can be used to generate all folded diagrams as indicated by the last three terms on the right-hand side of Eq. (5), where $\hat{Q}'$ is obtained from $\hat{Q}$ by removing all terms which are first order in the perturbing potential. When the folded diagrams are included, the disconnected valence diagrams such as diagram (d) of Fig. 1 will cancel among themselves. Similar techniques [7, 8] may be applied to evaluate the matrix elements of an operator.

The basic building blocks in any microscopic nuclear structure theory are thus these linked diagrams, and their evaluation is usually the first step in nuclear structure calculations. The purpose of the present paper is to devise a simple method to determine the angular momentum factors associated with such diagrams. In Section 2, we will first briefly review the ordinary diagram rules which are obtained from the Wick theorem and the anticommutation relations for fermions. These rules permit an easy evaluation of a diagram in the uncoupled representation or m-scheme, i.e. each fermion carries definite values for the z-components of the angular momentum and isospin. However, the nucleon–nucleon interaction is invariant under rotations in ordinary space and in isospin space and one should exploit this fact. Because of this, the fermion lines in diagrams should be coupled together to definite angular momentum J and isospin T. This leads to diagrams in the angular momentum coupled representation.

Hitherto, there seemed to be no simple systematic way of deriving the angular momentum factors associated with such diagrams, other than to start from the m-scheme, write out all the Clebsch–Gordan coefficients and perform the summations. This involves a great deal of angular momentum or Racah algebra and there is a significant possibility for error. As the example in the recent review of Ellis and Osnes [4] shows, the above procedure is complex even for the simple second-order core-polarization diagram. The third-order diagrams have been derived by Barrett and Kirson [9] using this approach, and in addition a few fourth-order ones were evaluated. However, the amount of Racah algebra necessary precludes detailed fourth-order studies. In fact to address this problem, Goode and Koltun [10] introduced the average interaction (averaged over J and T). Its calculation is then equivalent to that of the vacuum to vacuum diagrams and is thus computationally much simpler.

In Section 3 we will present a direct method for determining the angular momentum factors associated with linked Goldstone diagrams in the angular momentum coupled representation. Our method is general and can be used to evaluate effective interaction and/or effective operator diagrams of both closed-shell nuclei (vacuum to vacuum linked diagrams) and open-shell nuclei (valence linked diagrams). This allows one to write down the angular momentum factors of any diagram essentially by inspection. Obviously this can greatly simplify calculations and may allow one to tackle problems that would otherwise be intractable. Our method gives some attention to computer time considerations. In Section 4 we give a summary of our diagram rules and we evaluate a few representative diagrams to illustrate our technique.

2. Diagram Rules in the Uncoupled Representation

Using time-dependent perturbation theory [1, 2], the basic matrix elements which generate the model space effective interaction can be written as

$$M_{fi} = \langle C \mid A_f V(0) U(0, -\infty)\, A_i^\dagger \mid C \rangle_L , \tag{6}$$

where $\mid C\rangle$ is the closed-shell unperturbed ground state and L implies that we include only linked diagrams (valence linked diagrams in the case of valence nuclei). The time evolution operator $U(0, -\infty)$ is given by

$$U(0, -\infty) = \lim_{\substack{t' \to -\infty(1-i\epsilon) \\ \epsilon \to 0+}} \sum_{n=0}^{\infty} \left(\frac{-i}{\hbar}\right)^n \int_{t'}^{0} dt_1 \int_{t'}^{t_1} dt_2 \cdots \int_{t'}^{t_{n-1}} dt_n \, T[V(t_1) \cdots V(t_n)], \tag{7}$$

where T denotes the time-ordered product and all the perturbing operators $V(t)$ are in the interaction representation. For the ground state of closed-shell nuclei, $A_i^\dagger = A_f = 1$ and M_{fi} is just the sum of all the linked vacuum to vacuum diagrams such as diagram (a) of Fig. 1. For the case with valence particles and holes, $A_i^\dagger$ and A_f may have the form

$$\begin{aligned} A_i^\dagger &= a_1^\dagger a_3^\dagger a_2 , \\ A_f &= a_4^\dagger a_7^\dagger a_5 = (a_5^\dagger a_7^\dagger a_4)^\dagger . \end{aligned} \tag{8}$$

It may be noted that the ordering of the external lines is in accordance with the standard ordering chosen for the fermion operators in $A_i^\dagger$ and $A_f^\dagger$, as illustrated in Fig. 2. This will be the convention used in this work. With valence lines, the matrix element M_{fi} is just the sum of all the valence-linked (including folded) diagrams [1, 2] such as (c) and (e) of Fig. 1.

As each linked diagram is just a term in the perturbation expansion of the matrix element M_{fi}, as indicated by Eqs. (6) and (7), the starting point for the derivation of the diagram rules is clearly these two equations. In the uncoupled representation, the diagram rules can be readily derived from these two equations, using the Wick theorem and the symmetry properties of the operator $V(t)$. As they are well known (see, e.g., Refs. [3, 11, 12]), we will just state these rules in the following.

(i) From the time integrations of Eq. (7) we obtain an energy denominator factor

$$[\omega_i - (\Sigma \epsilon_p - \Sigma \epsilon_h)]^{-1} \tag{9}$$

between successive vertices. Here, ω_i is the starting energy, i.e., the unperturbed

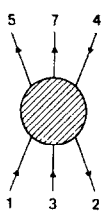

Fig. 2. Illustration of the ordering of external fermion lines discussed in the text.

energy at the time $t = -\infty$.[2] For example, $\omega_i = 0$ in Fig. 1a and $\omega_i = \epsilon_c - \epsilon_d$ in Fig. 1e. The ϵ's are the unperturbed single particle energies and we sum over all intermediate particle (p) and hole (h) indices between vertices, ignoring the exclusion principle. Note that our diagrams are time ordered (i.e., Goldstone diagrams) as indicated by the time constraints of Eq. (7).

(ii) For each vertex there is an antisymmetrized matrix element[3]

$$\langle ab \mid V \mid cd \rangle \equiv \langle ab \mid V \mid cd \rangle - \langle ab \mid V \mid dc \rangle, \tag{10}$$

where a and b "leave" the vertex from the left and right side and c and d "enter" the vertex from the left and right side, respectively. With this definition, the two-body interaction V may be written as

$$V = \tfrac{1}{4} \sum_{ijkl} \langle ij \mid V \mid kl \rangle \, a_i^\dagger a_j^\dagger a_l a_k \, . \tag{11}$$

In the uncoupled representation, the unperturbed wave functions used above are, for example, harmonic oscillator wave functions in the m-scheme. Thus $\mid d \rangle \equiv \mid (nljm, m_t)_d \rangle$.

We also need to deal with a one-body operator U, which may be a scalar operator in the perturbing potential or a tensor operator corresponding to an observable quantity. For each vertex U, there is a matrix element $\langle a \mid U \mid b \rangle$, where a leaves the vertex and b enters it. In the uncoupled representation, the operator U may be written as

$$U = \sum_{ij} \langle i \mid U \mid j \rangle \, a_i^\dagger a_j \, . \tag{12}$$

(iii) By applying the Wick theorem to Eqs. (6) and (7) we obtain for each diagram an overall factor of

$$(-1)^{n_h + n_l + n_c + n_{\text{exh}}} / 2^{n_{\text{ep}}}, \tag{13}$$

where n_h is the number of hole lines, n_l is the number of closed loops, n_c is the number of crossings of different external lines as they trace through the diagram, n_{exh} is the number of external hole lines which continuously trace through the diagram, including those which enter as hole lines but emerge as particle lines, and n_{ep} is the number of

[2] The starting energies for effective operator diagrams [7, 8] are slightly different. Because of the presence of two time evolution operators $U(\infty, 0)$ and $U(0, -\infty)$, the starting energy may be the unperturbed single particle energies at either $t = -\infty$ or $t = +\infty$, depending on the location of the time intervals. The operator acts at the time $t = 0$.

[3] The interaction V is in principle the free nucleon–nucleon interaction. However, since V generally contains a strong repulsive core, it is in actual calculations replaced by the more well-behaved nuclear reaction matrix G, which already includes the short-range correlations induced by V (see, e.g., Ref. [2]). As far as diagram rules are concerned, we may just replace the V vertices by the respective G vertices. This will be discussed further in Subsection 3.2 in connection with the particle–particle ladder diagrams.

pairs of lines which start at the same interaction, end at the same interaction and go in the same direction (so-called equivalent pairs).

Note that for external particle-hole lines, we should draw the particle lines to the left of the hole lines, as indicated in Eq. (8) and Fig. 2. The above rules are obtained with this convention. We will further comment on this point near the end of this section. We will now give some examples to illustrate the determination of the above factors. (These examples will also be used in Sections 3 and 4 to illustrate our rules for determining the angular momentum factors.)

The above rules are indeed simple and would enable one immediately to write down expressions for any linked Goldstone diagram in the uncoupled representation. To illustrate, we have for diagram (e) of Fig. 1

$$(1e) = \frac{(-1)^5}{2^0} \sum_{ph} \frac{\langle hd \mid V \mid pb \rangle \langle ap \mid V \mid ch \rangle}{(\epsilon_c - \epsilon_d) - (\epsilon_a + \epsilon_p - \epsilon_h - \epsilon_d)}, \tag{14}$$

where the overall factor results from

$$n_h = 3,\ n_l = 1,\ n_c = 0,\ n_{\text{exh}} = 1,\ n_{\text{cp}} = 0.$$

For the diagrams in Fig. 3, the values of the quantities n_h, n_l, etc., determining the overall factor (13) are given in Table I.

In (d), we seem to have a crossing of external lines, but this crossing is between the same external line. Thus $n_c = 0$. In (f) we have a crossing between two external lines. There are cases where $A_i^\dagger$ and A_f of Eq. (6) may not have the same number of fermion operators, as shown by diagram (h). This diagram arises in a model space calculation including one-particle and two-particle one-hole basis states. For such cases, it is indeed essential to follow the convention that in $A_i^\dagger$ and $A_f^\dagger$ we arrange the particle creation operators to the left of the hole creation operators. This is because of the following consideration. If $A_i^\dagger$ and $A_f^\dagger$ have the same number of fermion operators, then a similar rearrangement of these operators in both $A_i^\dagger$ and $A_f^\dagger$ will not alter

TABLE I

Values of Quantities Determining the Overall Factor for the Diagrams in Fig. 3

Diagram	n_h	n_l	n_c	n_{exh}	n_{cp}
(a)	4	3	0	0	1
(b)	4	3	0	0	2
(c)	3	1	0	0	2
(d)	3	2	0	0	1
(e)	4	1	0	2	1
(f)	2	1	1	0	0
(g)	2	2	0	0	0
(h)	1	0	0	1	1
(i)	1	1	0	0	0
(j)	0	0	0	0	1

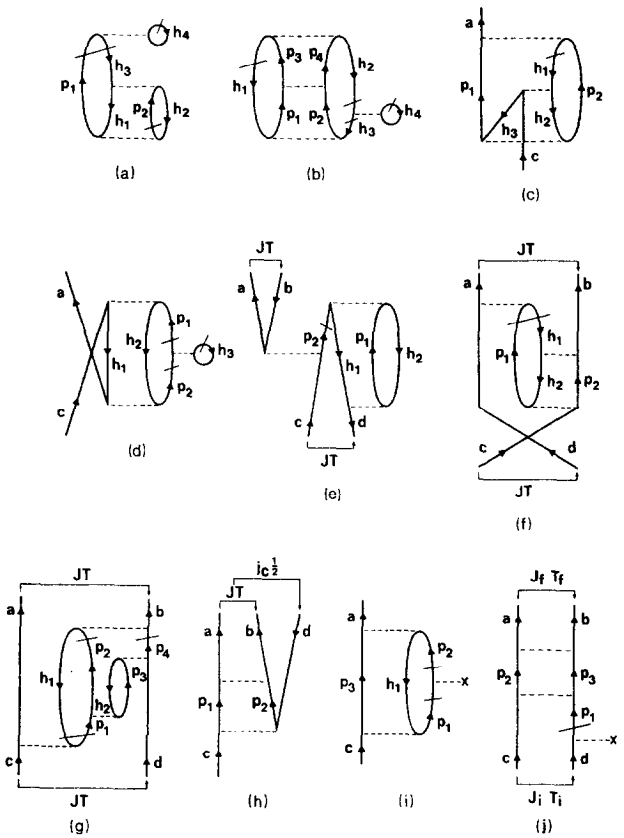

FIG. 3. Examples of effective interaction and operator diagrams.

the value of the diagram. Thus we have the freedom of, say, arranging all the hole creation operators in front of the particle creation operators in $A_i^\dagger$ and $A_f^\dagger$ and our diagram rules still apply. It is clear that we do not have such freedom if $A_i^\dagger$ and $A_f^\dagger$ do not have the same number of fermion operators.

Finally let us mention the familiar rule that from the set of exchange and topologically equivalent diagrams only one diagram is to be retained in the calculations. Such equivalent diagrams are easily identified by contracting the dashed-line vertex to a dot vertex (Hugenholtz notation). To illustrate, all the five diagrams of Fig. 4 are equivalent (i.e., they have the same value and correspond to the same physical process). Only one of them will be retained in actual calculations.

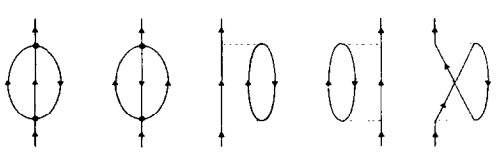

FIG. 4. Examples of equivalent diagrams.

3. Diagram Rules for the Coupled Representation

To determine the value of a given diagram, the rules given in Section 2 are first applied to obtain the energy denominators, factors, phases and the indices in the bra and ket vectors of the matrix elements involved. Our task here is to set out rules for determining the angular momentum couplings of these matrix elements, and associated factors, when the initial and final states of the diagram are coupled to a definite angular momentum and, if desired, isospin. In Subsection 3.1 we define various coupled matrix elements. In Subsection 3.2 we discuss the case of ladder diagrams (particle–particle, particle–hole or hole–hole ladders) since their angular momentum structure is particularly simple. Our strategy in the following subsections is then to express a given diagram in terms of ladder diagrams insofar as it is possible. In Subsection 3.3 we show that certain diagrams which are not in an obvious ladder form in the original coupling scheme, can be put into ladder form by angular momentum recoupling. As is explained, in order to perform the necessary recoupling transformations, it is convenient first to couple the diagram to a scalar. In Subsection 3.4 we show how other diagrams can be decomposed into products of ladder diagrams by cutting open internal lines. This technique can further be used to cut off one-body insertions, as discussed in Subsection 3.5. Then, in Subsection 3.6 we discuss the evaluation of diagrams for one-body tensor operators of rank greater than zero. Such diagrams are needed, for instance, if we wish to obtain matrix elements of the electromagnetic $E2$ operator so as to calculate the effective charge. Generalizations of our method to three-body cluster diagrams and other more complicated cases are discussed in Subsection 3.7.

3.1. *Cross-Coupled Matrix Elements*

In order to take full advantage of the power and flexibility of Racah algebra, it is worth realizing that in a two-particle matrix element the single-particle angular momenta can be coupled in several different ways.

First, we note that a single-particle ket vector $|jm\rangle$ transforms under rotation as a spherical tensor T_m^j of rank j, component m, while the corresponding bra vector $\langle jm|$ transforms as $(-1)^{j-m}T^j_{-m}$. Thus, we may define a coupled (unnormalized) two-particle ket vector as

$$|j_a j_b JM\rangle = \sum_{m_a m_b} C^{j_a\, j_b\, J}_{m_a m_b M} |(j_a m_a)(j_b m_b)\rangle$$

$$\equiv \{|j_a j_b\rangle\}^J_M , \tag{15}$$

which transforms as a spherical tensor T_M^J. In Eq. (15) C is a standard Clebsch–Gordan coefficient which is defined according to the Condon–Shortley phase convention. The corresponding bra vector is

$$\langle j_a j_b JM \mid = \sum_{m_a m_b} \langle (j_a m_a)(j_b m_b)\mid C^{j_a\, j_b\, J}_{m_a m_b M}$$

$$= \sum_{m_a m_b} \langle (j_a m_a)(j_b m_b)\mid (-1)^{j_a - m_a}(-1)^{j_b - m_b}(-1)^{J-M} C^{j_a\, j_b\, J}_{-m_a -m_b -M}$$

$$= (-1)^{J-M}\{\langle j_a j_b \mid\}^J_{-M}, \tag{16}$$

confirming that it transforms as a spherical tensor $(-1)^{J-M}T^J_{-M}$. Since the interaction operator V transforms as a scalar under rotation, the standard coupled (unnormalized) two-particle matrix element of V is given by

$$\langle j_a j_b JM \mid V \mid j_c j_d JM\rangle$$

$$= \sum_{m_a m_b m_c m_d} C^{j_a\, j_b\, J}_{m_a m_b M} C^{j_c\, j_d\, J}_{m_c m_d M} \langle (j_a m_a)(j_b m_b) \mid V \mid (j_c m_c)(j_d m_d)$$

$$= (-1)^{J-M} \sum_{m_a m_b m_c m_d} (-1)^{j_a - m_a}(-1)^{j_b - m_b} C^{j_a\, j_b\, J}_{-m_a -m_b -M} C^{j_c\, j_d\, J}_{m_c m_d M}$$

$$\times \langle (j_a m_a)(j_b m_b) \mid V \mid (j_c m_c)(j_d m_d)\rangle. \tag{17}$$

It follows from the Wigner–Eckart theorem that the matrix element is independent of M. The uncoupled matrix element on the right-hand side of Eq. (17) is antisymmetrized as stated in Section 2.

In the above we have suppressed the principal quantum numbers n and orbital angular momentum quantum numbers l which are not of relevance here. Further, it is not necessary to consider explicitly the isospin quantum numbers, since the isospin factors follow by replacing j and m by $\frac{1}{2}$ and m_t and by replacing J and M by T and M_T. (This is readily seen near the end of this subsection and in the examples of Section 4 where isospin factors are explicitly given.) Let us also replace j_a by a and m_a by α, etc., so that we simplify Eq. (17) to

$$\langle abJM \mid V \mid cdJM\rangle = \sum_{\alpha\beta\gamma\delta} C^{abJ}_{\alpha\beta M} C^{cdJ}_{\gamma\delta M} \langle (a\alpha)(b\beta) \mid V \mid (c\gamma)(d\delta)\rangle$$

$$\equiv \langle \overset{JM}{\underset{\downarrow}{\sqcap}}\, ab \mid V \mid cd \overset{JM}{\underset{\downarrow}{\sqcap}}\rangle. \tag{18}$$

Using well-known properties of Clebsch–Gordan coefficients we can reverse the direction of the coupling of the single-particle angular momenta on one or both sides of the matrix element, obtaining

$$\langle \overset{JM}{\underset{\downarrow}{\sqcap}}\, ab \mid V \mid cd \overset{JM}{\underset{\downarrow}{\sqcap}}\rangle = (-1)^{c+d-J} \langle \overset{JM}{\underset{\downarrow}{\sqcap}}\, ab \mid V \mid cd \overset{JM}{\underset{\downarrow}{\sqcap}}\rangle \tag{19}$$

and similar relations. Note that the ordering *abcd* is unchanged, only the direction of the coupling is altered.

As indicated at the beginning of this subsection, it will be convenient to consider alternative coupling schemes for the two-particle matrix elements. Thus, we shall

define "cross-coupled" matrix elements [13, 14] in which single-particle angular momenta from the bra and ket vectors are coupled, i.e., the coupling runs across the interaction operator. Two frequently encountered cross-coupled matrix elements are

$$\langle ab \mid V \mid cd \rangle_{JM} \equiv (-1)^{J-M} \sum_{\alpha\beta\gamma\delta} (-1)^{a-\alpha} C^{c\ \ a\ \ J}_{\gamma\ -\alpha\ -M} (-1)^{b-\beta} C^{d\ \ b\ \ J}_{\delta\ -\beta\ \ M} \langle (a\alpha)(b\beta) \mid V \mid (c\gamma)(d\delta) \rangle, \tag{20}$$

$$\langle ab \mid V \mid cd \rangle_{JM} \equiv (-1)^{J-M} \sum_{\alpha\beta\gamma\delta} (-1)^{a-\alpha} C^{d\ \ a\ \ J}_{\delta\ -\alpha\ -M} (-1)^{b-\beta} C^{c\ \ b\ \ J}_{\gamma\ -\beta\ \ M} \langle (a\alpha)(b\beta) \mid V \mid (c\gamma)(d\delta) \rangle, \tag{21}$$

which are defined in close analogy to Eq. (17). We emphasize that in each of Eqs. (20) and (21) the left-hand side should only be regarded as a short-hand notation for the expression given on the right-hand side. In both equations the phase factor $(-1)^{J-M}$ is included to ensure that the matrix elements are scalar and independent of M. We have chosen to associate the phase factor $(-1)^{J-M}$ and the value $-M$ of the total magnetic quantum number with the coupling involving the single-particle state a. This is of course arbitrary, since the matrix element is independent of M. Below we shall explicitly couple the total J's in Eqs. (20) and (21) to angular momentum zero, in which case the magnetic quantum numbers M and $-M$ do not show up at all.

This simple idea of cross-coupling is illustrated in Fig. 5. Diagram (a) corresponds to the ordinary coupled matrix element of Eq. (18). The cross-coupled matrix element of Eq. (20) corresponds to diagram (b), while the cross-coupled matrix element of Eq. (21) leads to diagram (c).

In the same way as for the standard coupled matrix elements we can reverse the direction of the coupling of the single-particle angular momenta in the cross-coupled matrix elements, obtaining

$$\langle ab \mid V \mid cd \rangle_{JM} = (-1)^{b+d-J} \langle ab \mid V \mid cd \rangle_{JM} \tag{22}$$

and similar relations. Again we note that the ordering *abcd* is unchanged, only the

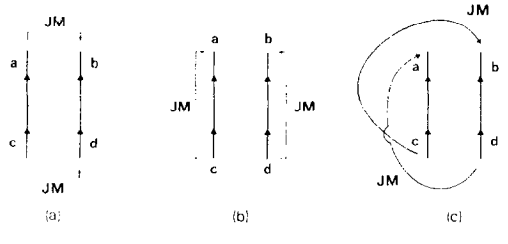

FIG. 5. Examples showing different ways of coupling matrix elements. If isospin couplings are also included, we just replace JM by $JMTM_T$.

direction of the coupling is reversed. In fact, we have as a general rule

$$\overset{\overset{JM}{\frown}}{\cdots a \cdots b \cdots} = (-1)^{a+b-J} \overset{\overset{JM}{\smile}}{\cdots a \cdots b \cdots}, \tag{23}$$

provided of course that the ordering of state labels remains unchanged.

The cross-coupled matrix elements (20) and (21) can be related to the standard coupled matrix element (17) or (18) and vice versa by means of angular momentum recoupling transformations. To that end it is useful explicitly to couple the matrix elements to scalars (as indicated below by the superscript 0). For the standard coupled matrix element (18) we have

$$\begin{aligned}
\overset{JM}{\langle}ab \mid V \mid \overset{JM}{cd\rangle} &= \hat{J}^{-2} \sum_M \overset{JM}{\langle}ab \mid V \mid \overset{JM}{cd\rangle} \\
&= \hat{J}^{-1} \sum_M (-1)^{J-M} C^{J\ J\ 0}_{M-M\ \ 0} \overset{JM}{\langle}ab \mid V \mid \overset{JM}{cd\rangle} \\
&= \hat{J}^{-1} \overset{J}{\langle}ab \mid V \mid \overset{J}{cd\rangle}^0,
\end{aligned} \tag{24}$$

where $\hat{J} \equiv \sqrt{2J+1}$. In the first step of Eq. (24) we used the fact that the matrix element is independent of M, while the second step was obtained using the well-known relation

$$C^{J\ J\ 0}_{M-M\ \ 0} = (-1)^{J-M} \hat{J}^{-1}. \tag{25}$$

We shall often refer to the scalar coupled matrix element on the right-hand side of Eq. (24) as a reduced matrix element. It is implied in Eq. (24) that the two-particle angular momenta are coupled in the order J_{in} (ket) to J_{out} (bra). Reversing this order gives rise to a phase $(-1)^{2J}$, which is of no consequence, since J is an integer.

Similarly, we can couple the total J's in the cross-coupled matrix elements (20) and (21) to zero resultant angular momentum, obtaining

$$\begin{aligned}
\underset{\underset{JM}{\frown}}{\overset{\overset{JM}{\smile}}{\langle}ab \mid V \mid cd\rangle} &= \hat{J}^{-2} \sum_M \overset{\overset{JM}{\smile}}{\langle}ab \mid V \mid \underset{\underset{JM}{\frown}}{cd\rangle} \\
&= \hat{J}^{-1} \sum_M (-1)^{J-M} C^{J\ J\ 0}_{M-M\ \ 0} \underset{\underset{JM}{\frown}}{\overset{\overset{JM}{\smile}}{\langle}ab \mid V \mid cd\rangle} \\
&= \hat{J}^{-1} \underset{\underset{J}{\frown}}{\overset{\overset{J}{\smile}}{\langle}ab \mid V \mid cd\rangle}^0,
\end{aligned} \tag{26}$$

$$\overbrace{\langle ab \mid V \mid cd\rangle}^{JM} = \hat{J}^{-1}\overbrace{\langle ab \mid V \mid cd\rangle^0}^{J}. \tag{27}$$

In Eq. (26) we have explicitly coupled the J's in the order J_{ab} to J_{ca}, although the order of the coupling may be reversed without changing the sign of the matrix element since J is an integer.

Now, using well-known recoupling transformations of Racah algebra, it is straightforward to relate reduced cross-coupled matrix elements to reduced standard coupled matrix elements. For example, we obtain for the reduced cross-coupled matrix elements on the right-hand sides of Eqs. (26) and (27)

$$\begin{aligned}\overbrace{\langle ab \mid V \mid cd\rangle^0}^{J} &= \sum_{J'} X\begin{pmatrix} d & b & J \\ c & a & J \\ J' & J' & 0 \end{pmatrix} \overset{J'}{\sqcap}\!\!\sqcap \langle ab \mid V \mid \overset{J'}{\sqcap}\!\!\sqcap cd\rangle^0 \\ &= \sum_{J'} X\begin{pmatrix} c & a & J \\ d & b & J \\ J' & J' & 0 \end{pmatrix} \overset{J'}{\sqcap}\!\!\downarrow \langle ab \mid V \mid \overset{J'}{\sqcap}\!\!\downarrow cd\rangle^0, \end{aligned} \tag{28}$$

$$\begin{aligned}\overbrace{\langle ab \mid V \mid cd\rangle^0}^{J} &= \sum_{J'} X\begin{pmatrix} c & b & J \\ d & a & J \\ J' & J' & 0 \end{pmatrix} \overset{J'}{\sqcap}\!\!\sqcap \langle ab \mid V \mid \overset{J'}{\sqcap}\!\!\downarrow cd\rangle^0 \\ &= \sum_{J'} X\begin{pmatrix} c & b & J \\ d & a & J \\ J' & J' & 0 \end{pmatrix} \overset{J'}{\sqcap}\!\!\downarrow \langle ab \mid V \mid \overset{J'}{\sqcap}\!\!\downarrow cd\rangle^0 (-1)^{a+b-J'} \\ &= \sum_{J'} X\begin{pmatrix} d & a & J \\ c & b & J \\ J' & J' & 0 \end{pmatrix} \overset{J'}{\sqcap}\!\!\downarrow \langle ab \mid V \mid \overset{J'}{\sqcap}\!\!\sqcap cd\rangle^0. \end{aligned} \tag{29}$$

Here, the X-coefficient is defined in terms of the Wigner 9-j symbol as

$$X\begin{pmatrix} r & s & t \\ u & v & w \\ x & y & z \end{pmatrix} = \hat{t}\hat{w}\hat{x}\hat{y}\begin{Bmatrix} r & s & t \\ u & v & w \\ x & y & z \end{Bmatrix}, \tag{30}$$

where we recall that $\hat{t} = \sqrt{2t+1}$.

Now, X-coefficients with zero arguments can be simplified. Some examples are

$$X\begin{pmatrix} r & s & t \\ u & v & t \\ x & x & 0 \end{pmatrix} = \hat{x}\hat{t}(-1)^{s+t+u+x}\begin{Bmatrix} r & s & t \\ v & u & x \end{Bmatrix}, \tag{31}$$

$$X\begin{pmatrix} r & r & 0 \\ u & u & 0 \\ x & x & 0 \end{pmatrix} = \hat{x}\hat{r}^{-1}\hat{u}^{-1}. \tag{32}$$

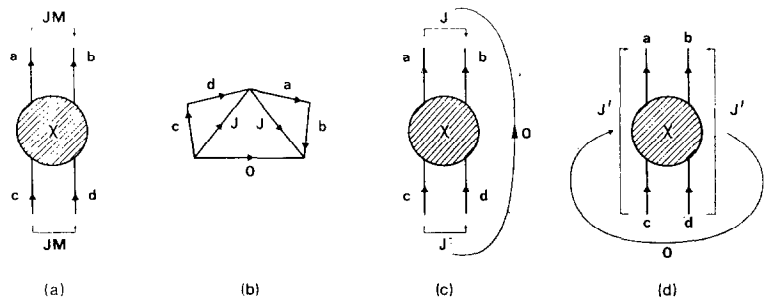

FIG. 6. Angular momentum couplings of a generalized vertex function.

On the right-hand side of Eq. (31) we have written a Wigner 6-j symbol. These expressions are useful in actual calculations. The angular momentum structure is most clearly displayed, however, by using the X-coefficient, so in most cases we shall not simplify the expressions we obtain.

Although we have only discussed the case of a single V interaction above, the same discussion can be applied to a product $\chi = VVV\cdots$, such as a $\hat{Q}$-box [12] composed of linked diagrams, since this also transforms as an angular momentum scalar. Thus for a given diagram, such as that shown in Fig. 6a, we first couple to zero resultant angular momentum as indicated in Figs. 6b and c, obtaining

$$\langle abJM \mid \chi \mid cdJM\rangle = \hat{J}^{-1}\langle \overset{J}{\overbrace{ab}} \mid \chi \mid \overset{J}{\overbrace{cd}}\rangle^{0}. \tag{33}$$

Hence, we need to evaluate the scalar coupled diagram of Fig. 6c and multiply by $\hat{J}^{-1}$. Having obtained the scalar coupled diagram, the cross coupling is easily performed. An example is shown in Fig. 6d corresponding to Eq. (28).

To summarize our developments thus far, we have associated factors

$$\langle \overset{JM}{\overbrace{ab}} \mid V \mid \overset{JM}{\overbrace{cd}}\rangle, \qquad \langle \overset{JM}{\overbrace{ab \mid V \mid cd}}\rangle \quad \text{and} \quad \langle \overset{JM}{\overbrace{ab \mid V \mid cd}}\rangle$$

with the diagrams in Figs. 5a, b and c, respectively. Further, as we have just seen, V may here be replaced by more complicated vertices χ containing any number of V

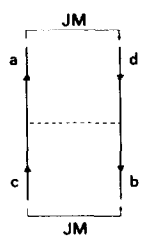

FIG. 7. Particle–hole diagram.

interactions. However, we have only considered particle–particle diagrams thus far. Then, turning to particle–hole diagrams, we may ask whether similar rules hold. Consider, for example, the particle–hole diagram shown in Fig. 7 corresponding to the matrix element $\langle ad^{-1}JM \mid V \mid cb^{-1}JM\rangle$. The angular momentum coupling is similar to that of the particle–particle diagram shown in Fig. 5c (except for the direction of the coupling between a and d). However, the detailed tensorial character of the coupling between a and d is different in the two cases, such that

$$\langle ad^{-1}JM \mid V \mid cb^{-1}JM\rangle = (-1)^{2d} \overbrace{\underbrace{\langle ab \mid V \mid cd\rangle}}^{JM}. \tag{34}$$

Here we are only considering the angular momentum structure of the respective diagrams. The phase factors due to contractions of fermion operators have already been taken care of in Section 2.

The origin of the phase in Eq. (34) is seen by coupling the particle and hole spherical tensors T^a and $T^{d\dagger}$ according to

$$\overbrace{T^a T^{d\dagger}}^{JM} = \sum_{\alpha\delta} C^{a\ d\ J}_{\alpha-\delta\ M} (-1)^{d-\delta}\, T^a_\alpha T^{d\dagger}_\delta. \tag{35}$$

Then, taking the Hermitian conjugate of both sides, we obtain

$$\overbrace{(T^a T^{d\dagger})^\dagger}^{JM} = (-1)^{2d+J-M} \overbrace{T^d T^{a\dagger}}^{J-M}. \tag{36}$$

Here, the left-hand side describes the angular momentum properties of the bra vector $\langle ad^{-1}JM \mid$ appearing in the particle–hole matrix element on the left-hand side of Eq. (34). Further, except for the phase $(-1)^{2d}$, the right-hand side of Eq. (36) describes the angular momentum coupling between a and d in the cross-coupled matrix element on the right-hand side of Eq. (34). Hence, relation (34) results. It is instructive to contrast Eq. (36) with the relation

$$\overbrace{(T^a T^d)^\dagger}^{JM} = (-1)^{J-M} \overbrace{T^{d\dagger} T^{a\dagger}}^{J-M}, \tag{37}$$

which describes the tensorial character of a particle–particle bra vector and is thus equivalent to Eq. (16), above.

The difference between the coupling schemes employed on the left- and right-hand sides of Eq. (34) may be further illustrated by considering the explicit expressions for the coupled matrix elements in terms of the uncoupled ones, namely,

$$\langle ad^{-1}JM \mid V \mid cb^{-1}JM\rangle = \sum_{\alpha\beta\gamma\delta} C^{a\ d\ J}_{\alpha-\delta\ M} C^{c\ b\ J}_{\gamma-\beta\ M} (-1)^{d-\delta}(-1)^{b-\beta} \langle (a\alpha)(b\beta) \mid V \mid (c\gamma)(d\delta)\rangle, \tag{38}$$

$$\overbrace{\langle ab \mid V \mid cd\rangle}^{JM} = (-1)^{J-M} \sum_{\alpha\beta\gamma\delta} C_{-\alpha\ \delta-M}^{a\ d\ J} C_{\gamma-\beta\ M}^{c\ b\ J} (-1)^{a-\alpha}(-1)^{b-\beta} \underbrace{\langle (a\alpha)(b\beta) \mid V \mid (c\gamma)(d\delta)\rangle}_{JM}. \tag{39}$$

Again, in writing Eq. (38) we have ignored the phase factors due to contractions of fermion operators, since we are only interested here in the angular momentum structure of the diagrams. We now observe that in Eq. (38) the phase factors $(-1)^{j-m}$ are always associated with *hole* lines, whereas in Eq. (39) they are always associated with *outgoing* lines. Thus, an outgoing hole line in the particle–hole coupling scheme (38) is treated similarly to an outgoing particle line in the particle–particle coupling scheme (39). On the other hand, an incoming hole line in the particle–hole scheme is treated differently from an incoming particle line in the particle–particle scheme. Now, our diagram rules will always be expressed in terms of angular momentum couplings among *particle* lines only, as was done, for example, in Eq. (39). Thus, in such a scheme we have to associate a phase factor $(-1)^{2h}$ with a particle–hole pair ph^{-1} on the top (bra) side of the diagram.

This can easily be generalized, so that for each complete diagram, which is expressed in terms of particle–particle coupled interaction vertices (matrix elements), we obtain a phase factor

$$(-1)^{n_{\mathrm{tph}}}, \tag{40}$$

where n_{tph} is the number of particle-hole pairs on the top (bra) side of the diagram. We emphasize that this phase is due to the particular coupling scheme of Eq. (35) chosen for external particle and hole lines, namely,

$$A_i^\dagger = \sum_{m_p m_h} (-1)^{h-m_h} C_{m_p-m_h\ M}^{p\ h\ J} a_{pm_p}^\dagger a_{hm_h}$$

and similarly for $A_f{}^\dagger$. Then, A_f is defined according to Eq. (36) as $A_f = (A_f{}^\dagger)^\dagger$.[4] Further, we note that the phase arises from angular momentum considerations. Thus, the phase arises twice if we couple both angular momentum and isospin, i.e.,

$$(-1)^{2h} \to (-1)^{2(j_h+1/2)} = +1, \tag{41}$$

and in this case the phases in Eqs. (34) and (40) can simply be ignored.

Finally, let us point out that in actual calculations the coupled matrix elements needed are in fact of the following three basic types:

$$\overset{JT}{\langle ab \mid V \mid cd\rangle}^{00}, \qquad \overbrace{\langle ab \mid V \mid cd\rangle}^{JT\ \ JT\ \ 00} \qquad \text{and} \qquad \overbrace{\langle ab \mid V \mid cd\rangle}^{JT\ \ JT\ \ 00}, \tag{42}$$

[4] Note that Eq. (36) implies that scalar coupled matrix elements be constructed according to our standard rule [see comments following Eqs. (24) and (25)], by coupling the external state with lines entering vertices to the external state with lines leaving vertices. If both particles and holes are present, particle–hole pairs may be ignored in determining the coupling order (this implies that if initial and final states involve only particle–hole pairs, the order of coupling is arbitrary).

where both ordinary angular momenta and isospins are coupled. The superscript 00 implies the coupling of both angular momenta and isospins to a total of zero. The transformation relations among the matrix elements (42) involve straightforward generalizations of Eqs. (28) and (29). For example, corresponding to Eq. (28) we have

$$\overbrace{\langle ab \mid V \mid cd\rangle}^{JT\ 00} = \sum_{J'T'} X \begin{pmatrix} c & a & J \\ d & b & J \\ J' & J' & 0 \end{pmatrix} X \begin{pmatrix} \frac{1}{2} & \frac{1}{2} & T \\ \frac{1}{2} & \frac{1}{2} & T \\ T' & T' & 0 \end{pmatrix} \overbrace{\langle ab \mid V \mid cd\rangle}^{J'T'\ J'T'}{}^{00}. \tag{43}$$

3.2. *Ladder Diagrams*

Our strategy is now to decompose a given diagram into products of ladders which have very simple angular momentum structure. An example of a particle–particle ladder is given in Fig. 8a. Figures 8b and c give alternative forms for a particle–hole ladder; the diagrams are actually equivalent, as can be seen by contracting the dashed line to a dot. Backward going vertices can also be included so that Fig. 8d is also a ladder. Hole–hole ladders can be treated similarly, although we do not give an explicit example.

Let us study the angular momentum structure of ladders in some detail. First, consider the simple particle–particle ladder shown in Fig. 9a. We note that angular momentum couplings are imposed on the external lines, in accordance with Eq. (17). For the internal lines we sum freely over all m-states. Then, keeping the p_1 and p_2 of the intermediate states fixed and disregarding the energy denominator (9) and overall factor (13) associated with the corresponding uncoupled diagram, we obtain

$$\begin{aligned} \text{Diagram 9a} &= \sum_{\alpha\beta\gamma\delta} (-1)^{a-\alpha}(-1)^{b-\beta}(-1)^{J-M} C_{-\alpha-\beta-M}^{a\ b\ J} C_{\gamma\ \delta\ M}^{c\ d\ J} \\ &\quad \times \sum_{m_1 m_2} \langle (a\alpha)(b\beta) \mid V \mid (p_1 m_1)(p_2 m_2)\rangle\langle (p_1 m_1)(p_2 m_2) \mid V \mid (c\gamma)(d\delta)\rangle \\ &= \hat{p}_1 \hat{p}_2 \overbrace{\langle ab \mid V \mid \overbrace{p_1 p_2\rangle\langle p_1 p_2}^{00} \mid V \mid cd\rangle}^{JM}. \end{aligned} \tag{44}$$

In obtaining the coupling of the internal lines on the right-hand side of Eq. (44), we used the relation

$$\sum_m |jm\rangle\langle jm| = j \sum_m (-1)^{j-m} C_{m-m\ 0}^{j\ j\ 0} |jm\rangle\langle jm| = \hat{j} \{|j\rangle\langle j|\}_0^0 \equiv \hat{j} \overbrace{|j\rangle\langle j|}^{00}. \tag{45}$$

Thus, each internal line may be regarded as being cut into two pieces which are coupled to zero resultant angular momentum, as shown in Fig. 9b. Further, the order of the coupling is such that the incoming piece of the internal line (i.e., the piece entering a vertex) is coupled to the outgoing piece (i.e., the piece leaving a vertex). Now, such a cross-channel coupling of the internal lines has the disadvantage

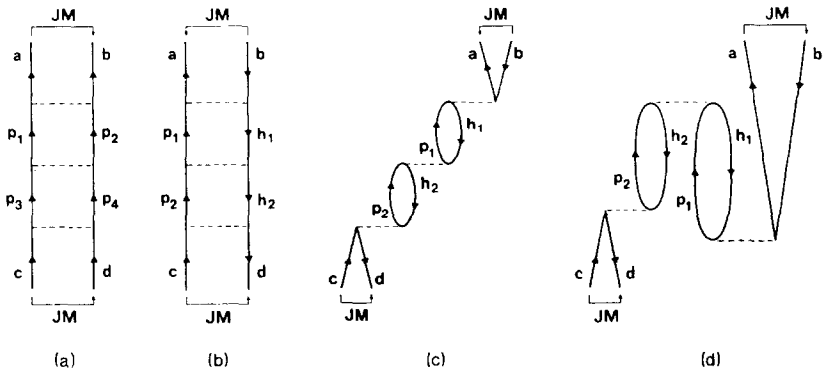

FIG. 8. Ladder diagrams.

that is connects *different* matrix elements, which is clearly inconvenient from a computational point of view. However, by a simple recoupling transformation we can change the scheme of coupling such that internal lines belonging to the same matrix element are coupled together. Using the transformation

$$\hat{r}\hat{s}\,|\,rs\rangle\langle rs\,| = \hat{r}\hat{s}\sum_{J'} X\begin{pmatrix} r & r & 0 \\ s & s & 0 \\ J' & J' & 0 \end{pmatrix}\{|\,rs\rangle\langle rs\,|\}^0_0 = \sum_{J'}\hat{J}'\{|\,rs\rangle\langle rs\,|\}^0_0 = \sum_{J'M'}|\,rs\rangle\langle rs\,| \quad (46)$$

in Eq. (44), we obtain the obvious and well-known result

$$\text{Diagram 9a} = \langle ab\,|\,V\,|\,p_1p_2\rangle\langle p_1p_2\,|\,V\,|\,cd\rangle. \quad (47)$$

This expression clearly shows the simplicity of the angular momentum structure of

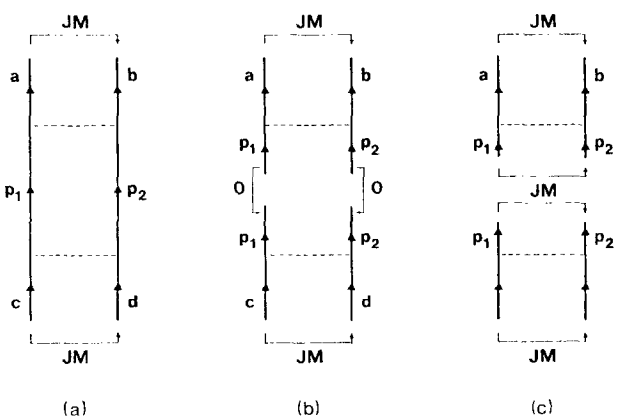

FIG. 9. Factorization of a particle–particle ladder diagram.

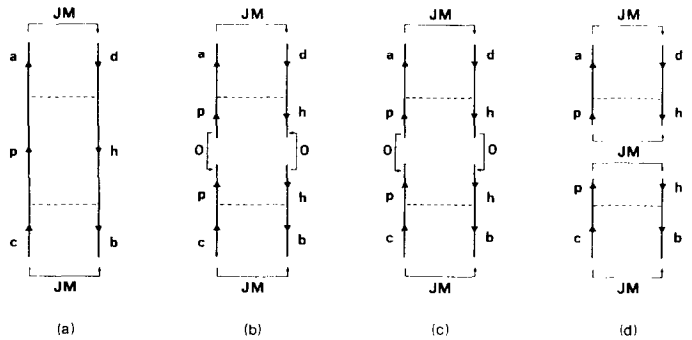

FIG. 10. Factorization of a particle–hole ladder diagram.

ladder diagrams. This simplicity lies in the fact that the J and M of the initial coupling imposed on the external lines is conserved throughout the sequence of interactions. Thus, a ladder diagram is expressed as a simple product of matrix elements of the interaction vertices, all with the same J and M, as illustrated in Fig. 9c.

In passing we note that the nuclear G-matrix, which is a basic concept in nuclear structure calculations with realistic forces, is simply given by the sum of all particle–particle ladders. Thus, the angular momentum structure of the G-matrix is uniquely determined by the total J and T of the external lines, which are conserved throughout the sequence of V interactions. We can express our diagrams in terms of G vertices by replacing V by G everywhere and, to avoid double counting, leaving out diagrams with particle–particle intermediate states between successive G vertices. However, it may be argued that *low-energy* intermediate states should be excluded from G and treated explicitly as particle–particle ladders in G (see, e.g., Ref. [4]).

It may seem that we have worked unnecessarily hard for the above trivial results. Our efforts are not wasted, however, as they have prepared us for treating the more subtle case of particle–hole ladders. Consider the simple second-order particle–hole ladder shown in Fig. 10a. The external lines are coupled to given J and M according to definition (38), while for the internal lines we sum freely over all the m-states. Thus, in a fashion similar to that used for the particle–particle ladder in Eq. (44), we obtain for the particle–hole ladder of Fig. 10a, keeping the p and h of the intermediate states fixed and disregarding the energy denominator (9) and the overall factor (13) of the corresponding uncoupled diagram

$$\text{Diagram 10a} = \sum_{\alpha\beta\gamma\delta} (-1)^{d-\delta}(-1)^{b-\beta} C^{a\ d\ J}_{\alpha-\delta\ M} C^{c\ b\ J}_{\gamma-\beta\ M}$$

$$\times \sum_{m_p m_h} \langle (a\alpha)(hm_h) \mid V \mid (pm_p)(d\delta)\rangle\langle (pm_p)(b\beta) \mid V \mid (c\gamma)(hm_h)\rangle$$

$$= (-1)^{2d}\, \hat{p}\hat{h}\langle ah \mid V \mid pd\rangle\langle pb \mid V \mid ch\rangle. \qquad (48)$$

(JM, JM; 00; 00)

Here, we have used Eq. (34) for the coupling of the external lines; the phase $(-1)^{2d}$ is thus associated with the top particle–hole pair, as discussed in the previous subsection. The coupling scheme of the internal lines is illustrated in Fig. 10b. We note that here we have followed the convention for the order of coupling defined in Eq. (45), namely that the incoming part of an internal line is coupled to the outgoing part. This has the consequence that in Fig. 10b the upper part of the diagram is coupled to the lower part via the particle line, while the lower part is coupled to the upper part via the hole line. This "hybrid" coupling scheme is clearly not so convenient for making the recoupling transformation in the intermediate states necessary for factorization on the right-hand side of Eq. (48). In order to perform this transformation, which is similar to that of Eq. (46) employed for the particle–particle ladder, the direction of coupling must be the same for both internal lines. To achieve this, we choose to reverse the direction of coupling for the internal *hole* line. This reversal of the coupling, which is illustrated in Fig. 10c, clearly gives a phase factor $(-1)^{2h}$. Then, we can apply the transformation (46) to rewrite Eq. (48) as

$$\text{Diagram 10a} = (-1)^{2d}(-1)^{2h}\langle ah \mid V \mid pd\rangle\langle pb \mid V \mid ch\rangle. \tag{49}$$

This factorization, which is illustrated in Fig. 10d, is similar to that obtained for the particle–particle ladder. There are, however, phase differences. Firstly, there is a phase factor $(-1)^{2d}$ associated with the top particle–hole pair, as explained in the previous subsection. We emphasize that this phase only arises if the particle–hole ladder is a complete diagram by itself. As we shall eventually see, ladders may also be considered as internal building blocks of more complex diagrams. In such cases the external legs of the particle–hole ladder will be internal lines of the complete diagram and will furthermore be coupled according to Eq. (39), which is the appropriate coupling scheme for our diagram rules, and thus the phase $(-1)^{2d}$ will not arise. Further discussion of this point is given in Subsection 3.4. Secondly, there is a phase factor $(-1)^{2h}$ associated with the internal particle–hole pair cut open. Both these phase factors arise from angular momentum considerations. In addition there are phase and overall factors not shown here coming from the contractions of fermion operators in the corresponding uncoupled diagram, as discussed in Section 2.

To summarize, we have just shown the need for a phase factor

$$(-1)^{n_{ph}}, \tag{50}$$

where n_{ph} is the number of internal particle–hole pairs cut open for which the particle and hole lines are coupled in the *same* direction across the cut, e.g., $n_{ph} = 1$ in Fig. 10c. The above phase rule will be further discussed in Subsection 3.4. As was the case for the phase factor (40), the phase factor (50) is associated with the coupling of ordinary angular momenta only. If the isospins are coupled as well, this phase arises twice as shown in Eq. (41), and can thus simply be ignored.

We are now able to evaluate more complicated ladder diagrams merely by inspection. Consider for example the third-order ladders shown in Fig. 8. We shall not consider isospin and only be concerned with the angular momentum structure of the diagrams. Thus, as before we shall keep the j-values of the intermediate states fixed and ignore the energy denominators and the overall factors associated with the corresponding uncoupled diagrams. Then, applying the rules of this and the previous subsection we immediately have

$$\text{Diagram 8a} = \overset{JM}{\langle} ab \mid V \mid p_1 p_2 \overset{JM}{\rangle\langle} p_1 p_2 \mid V \mid p_3 p_4 \overset{JM}{\rangle\langle} p_3 p_4 \mid V \mid cd \overset{JM}{\rangle}, \tag{51}$$

$$\text{Diagram 8c} = (-1)^3 \overset{JM}{\langle} h_1 a \mid V \mid p_1 b \overset{JM}{\rangle\langle} h_2 p_1 \mid V \mid p_2 h_1 \overset{JM}{\rangle\langle} dp_2 \mid V \mid ch_2 \overset{JM}{\rangle}, \tag{52}$$

$$\text{Diagram 8d} = (-1)^3 \overset{JM}{\langle} h_2 h_1 \mid V \mid p_2 p_1 \overset{JM}{\rangle\langle} dp_2 \mid V \mid ch_2 \overset{JM}{\rangle\langle} p_1 a \mid V \mid h_1 b \overset{JM}{\rangle}. \tag{53}$$

The phases in Eqs. (52) and (53) arise from the fact that the corresponding diagrams each have one particle–hole pair on the top and two internal particle–hole pairs. We note that the order of coupling of the intermediate angular momenta must be consistent, implying for example that p_1 must couple to h_1 in both matrix elements. Further, the external legs are coupled to angular momentum J according to the chosen convention. For example, in diagram 8c the direction of the coupling for c and d is from c to d, while for a and b it is from b to a.

Note that this procedure can be applied to generalized ladder diagrams for which the rungs of the ladder may be of more complex structure than a single V interaction. We may use the notation χ of Fig. 6 and Eq. (33) for such complex rungs. The analysis

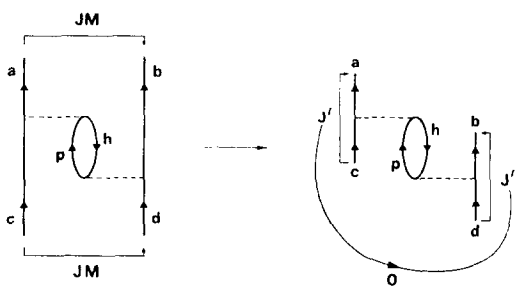

FIG. 11. Recoupling of the core-polarization diagram.

of this subsection then serves to break the diagram into a product of coupled matrix elements of χ, which must then be evaluated by the techniques described in the following subsections.

3.3. *Recognizing Ladders*

Sometimes in the original coupling scheme the diagram (or part of a diagram) is not in an obvious ladder form, but can be put into the desired ladder form by angular momentum recoupling. A simple example is the core-polarization diagram of Fig. 11a. The diagram is first coupled to a scalar and then transformed to the cross-coupled scheme indicated in Fig. 11b. This is evidently of ladder form so that the method of Subsection 3.2 can be used. Thus, we obtain, ignoring as before the phases and factors of the corresponding uncoupled diagram discussed in Section 2:

$$\text{Diagram 11a} = \hat{J}^{-1} \sum_{J'} X \begin{pmatrix} c & d & J \\ a & b & J \\ J' & J' & 0 \end{pmatrix} \overbrace{\langle ab \mid \chi \mid cd \rangle^0}^{J'}_{J'}$$

$$= (-1)^1 \hat{J}^{-1} \sum_{J'} X \begin{pmatrix} c & d & J \\ a & b & J \\ J' & J' & 0 \end{pmatrix} \hat{J}' \overbrace{\langle ah \mid V \mid cp \rangle}^{J'M'}_{J'M'} \overbrace{\langle pb \mid V \mid hd \rangle}^{J'M'}_{J'M'}. \quad (54)$$

In the second step of Eq. (54) we used the phase rule (50). This expression is identical to that derived by Osnes *et al.* [14]. Bertsch [19] has also obtained an expression of this form using essentially the same method that we present here. (He only discusses the evaluation of this particular diagram, however.) Further, it is easily shown by applying Eqs. (22), (28) and (31) that this expression is equivalent to those obtained by Barrett and Kirson [9] and by Ellis and Osnes [4]. The present expression, however, has the advantage that, once the cross-coupled matrix elements are calculated, a single summation over J' is required, whereas the other forms are written as a summation over three J's. Thus, our expression is not only easy to derive, but is immediately in a transparent form which is suitable for efficient computation.

3.4. *Decomposition of Diagrams into Ladders by Cutting Internal Lines*

There are diagrams (or parts of a diagram) which can be put into the form of ladders by judiciously cutting open one or more internal lines. This technique was in fact already used in Subsection 3.2 to factorize ladder diagrams. According to Eq. (45) an internal line consists of two pieces (an incoming one and an outgoing one) which are coupled together to a scalar in the cross channel. This coupling can then be broken by a suitable recoupling transformation. As an example, consider the diagram shown in Fig. 12a, which is apparently not of ladder form. First, we couple the external legs to a scalar. Then, if we apply Eq. (45) to the internal line p_1 (corresponding to cutting this line), we obtain the diagram shown in Fig. 12b. Here, both angular momentum couplings run from an incoming line to an outgoing line, in accordance with our

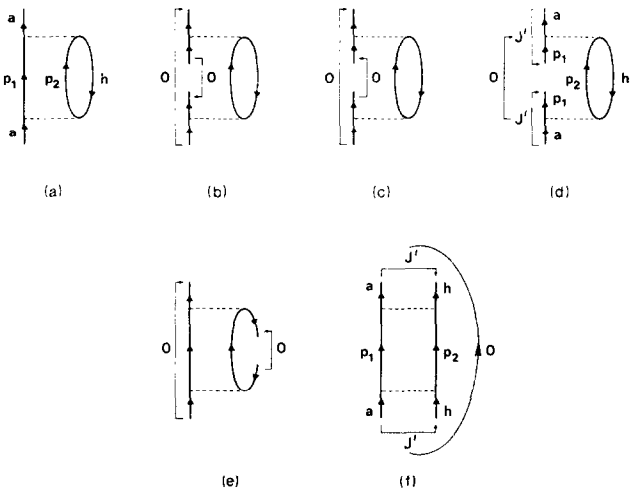

FIG. 12. Examples of cutting internal lines.

convention. Thus, the arrows of the two couplings point in opposite directions. This situation is similar to that encountered in Eq. (48) for the particle–hole ladder and is not convenient for performing the desired recoupling transformation leading to the diagram of Fig. 12d. To prepare for this recoupling, we reverse the direction of coupling for the internal line, as shown in Fig. 12c. This clearly gives rise to a phase $(-1)^{2p_1}$. Then, it is straightforward to make the recoupling transformation to diagram (d), which is of the desired ladder form. Following these steps, it is trivial to write down the expression for the diagram of Fig. 12a. We obtain, ignoring as before all the factors associated with the uncoupled diagram and keeping the j-values of the internal lines fixed:

$$\text{Diagram 12a} = \hat{a}^{-1}\hat{p}_1(-1)^{2p_1}\sum_{J'} X\begin{pmatrix} a & a & 0 \\ p_1 & p_1 & 0 \\ J' & J' & 0 \end{pmatrix} \overbrace{\underbrace{\langle ap_1 \mid \chi \mid p_1 a\rangle^0}_{J'}}^{J'} \tag{55a}$$

$$= \hat{a}^{-1}\hat{p}_1(-1)^{2p_1}\sum_{J'} X\begin{pmatrix} a & a & 0 \\ p_1 & p_1 & 0 \\ J' & J' & 0 \end{pmatrix} \hat{J}'(-1)^{2h}\overbrace{\underbrace{\langle ah \mid V \mid p_1 p_2\rangle}_{J'M'}}^{J'M'}\overbrace{\underbrace{\langle p_1 p_2 \mid V \mid ah\rangle}_{J'M'}}^{J'M'} \tag{55b}$$

$$= \hat{a}^{-2}(-1)^{2p_1}(-1)^{2h}\sum_{J'} \hat{J}'^2\overbrace{\underbrace{\langle ah \mid V \mid p_1 p_2\rangle}_{J'M'}}^{J'M'}\overbrace{\underbrace{\langle p_1 p_2 \mid V \mid ah\rangle}_{J'M'}}^{J'M'}. \tag{55c}$$

In Eq. (55a) the factors $\hat{a}^{-1}$ and $\hat{p}_1$ are associated with the step from diagram (a) to diagram (b). The further step to diagram (c) gives the phase $(-1)^{2p_1}$, while the X-coefficient takes care of the transformation from diagram (c) to diagram (d). The matrix element of χ is simply short-hand notation for diagram (d) and is written out in

detail in Eq. (55b). Here, the factor $\hat{J}$ follows from uncoupling the scalar coupled matrix element of χ, while the phase $(-1)^{2h}$ follows by the rule (50) from cutting the intermediate particle–hole pair of the ladder. Finally, by substituting expression (32) for the X-coefficient, we obtain Eq. (55c).

Now, the present technique is not unique as a given diagram can often be put into different ladder forms by cutting different internal lines. The final result must of course be the same in all cases, and thus one may choose the procedure leading to the simplest calculation. For example, the diagram of Fig. 12a can also be put into ladder form by cutting the internal hole line h, as shown in Fig. 12e. This diagram can then be transformed to the particle–particle ladder of Fig. 12f by straightforward angular momentum recoupling. Note that in Fig. 12f we have, for clarity, opened out the h lines; internal lines may be twisted at will when evaluating the angular momentum structure of a diagram, provided that the direction of the arrow (toward or away from the vertex) is maintained. By this procedure we readily obtain for the diagram of Fig. 12a

$$\text{Diagram 12a} = \hat{a}^{-1}\hat{h}\sum_{J'} X\begin{pmatrix} a & a & 0 \\ h & h & 0 \\ J' & J' & 0 \end{pmatrix} \langle ah \mid \chi \mid ah\rangle^0$$

$$= \hat{a}^{-2}\sum_{J'} \hat{J}'^2 \langle ah \mid V \mid p_1 p_2\rangle\langle p_1 p_2 \mid V \mid ah\rangle. \tag{56}$$

This expression must of course be equivalent to that of Eq. (55). This is in fact easily shown by applying Eqs. (23), (26), (28), (24) and the orthogonality relation for X-coefficients to Eq. (55). Comparing the two procedures, it is apparent that the procedure leading to Eq. (56) is slightly simpler and more convenient for computation than that leading to Eq. (55).

The present example serves to illustrate the meaning of the phase rule (50). In fact, the phase factor $(-1)^{n_{ph}}$ is associated with cut particle–hole pairs only. Thus, it is not unique for a given diagram, but depends on how it is evaluated. In Eq. (55) the original diagram was expressed in terms of a particle–hole ladder, while in Eq. (56) it was expressed in terms of a particle–particle ladder. Thus, the phase rule $(-1)^{n_{ph}}$ only applies to the evaluation of the particle–hole ladder in Eq. (55).

As another example, consider the simple third-order ring diagram shown in Fig. 13a. We cut the lines labelled p_1 and h_1, as shown in Fig. 13b. Since the coupling across p_1 is in the opposite direction to the coupling across h_1, we reverse the latter as shown in Fig. 13c, obtaining a phase $(-1)^{2h_1}$. Then we perform a straightforward recoupling transformation to obtain the diagram of Fig. 13d, which is in the form of a scalar coupled particle–hole ladder. Writing down these steps in algebraic form, we readily obtain

$$\text{Diagram 13a} = \hat{p}_1\hat{h}_1(-1)^{2h_1}\sum_{J'} X\begin{pmatrix} p_1 & p_1 & 0 \\ h_1 & h_1 & 0 \\ J' & J' & 0 \end{pmatrix} \langle h_1 p_1 \mid \chi \mid p_1 h_1\rangle^0, \tag{57}$$

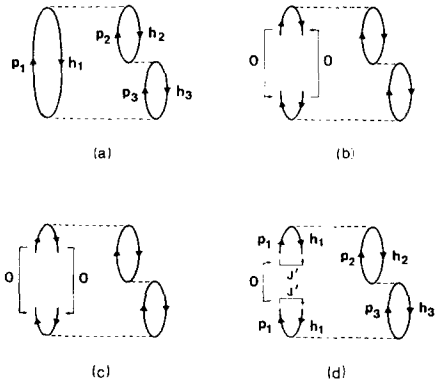

FIG. 13. Example of cutting internal lines.

where the scalar coupled particle–hole ladder is easily evaluated by the rules of Subsection 3.2:

$$\langle h_1 p_1 \mid \chi \mid p_1 h_1 \rangle^0 = (-1)^{2h_2+2h_3}\, \hat{J}' \langle h_1 h_2 \mid V \mid p_1 p_2 \rangle \langle p_2 h_3 \mid V \mid h_2 p_3 \rangle \langle p_1 p_3 \mid V \mid h_1 h_3 \rangle. \tag{58}$$

Note that h_1 is an internal hole line, so that the phase rule (40) does not apply to the

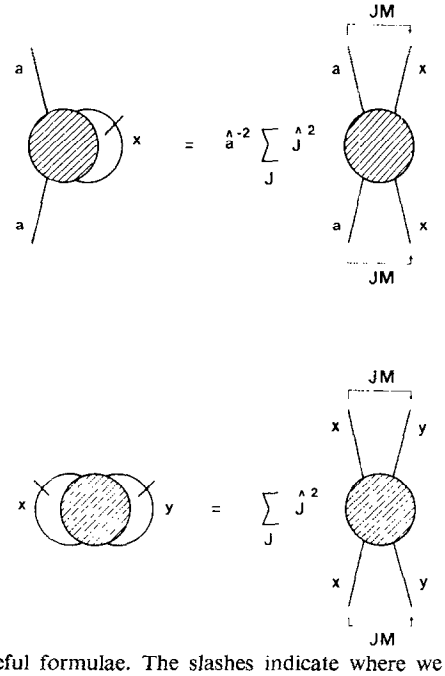

FIG. 14. Some useful formulae. The slashes indicate where we have cut the lines.

evaluation of the particle–hole ladder in Eq. (58). This is because the coupling between p_1 and h_1 is not externally imposed, but results from suitable recoupling of the internal lines. This coupling is automatically expressed in the appropriate scheme, and the phase rule (40) is not of relevance here. The phases on the right-hand sides of Eqs. (57) and (58) follow from the rule (50) since we cut in all three particle–hole pairs.

The present technique is schematically illustrated in Fig. 14. Note here that the lines may be either particle or hole lines. To obtain correct phases the lines on the right-hand side of the figure should be regarded as external lines. The rules of Fig. 14 are also obeyed if the single lines labelled a, x and y each actually represent several lines coupled to total angular momenta of a, x and y, respectively.

In the examples considered above, the lines were cut horizontally. However, we often wish to cut lines vertically, as indicated in Fig. 15. Note that the number of lines in the upper part of the cut must be the same as the number of lines in the lower part. A vertical cut can obviously be viewed as two horizontal cuts, and recoupling transformations can then be used to write the diagram in the desired form. As an example, consider the diagram shown in Fig. 16a. We first couple the diagram to a scalar and recouple it to cross-coupled form (Fig. 16b). Then, we cut the lines h_1 and h_2, as indicated in Fig. 16c. A final recoupling transformation serves to factorize the original diagram into the diagrams shown in Figs. 16d and e. Picking up the phases and factors from these operations we readily obtain

$$\text{Diagram 16a} = \hat{J}^{-1} \sum_{J'} X \begin{pmatrix} c & d & J \\ a & b & J \\ J' & J' & 0 \end{pmatrix} (-1)^{2h_1} \hat{h}_1 \hat{h}_2 X \begin{pmatrix} h_2 & h_2 & 0 \\ h_1 & h_1 & 0 \\ J' & J' & 0 \end{pmatrix} X \begin{pmatrix} J' & J' & 0 \\ J' & J' & 0 \\ 0 & 0 & 0 \end{pmatrix}$$

$$\times \langle a h_1 \mid \chi \mid c h_2 \rangle^0 \langle h_2 b \mid V \mid h_1 d \rangle^0$$

$$= (-1)^{2h_1} \hat{J}^{-1} \sum_{J'} X \begin{pmatrix} c & d & J \\ a & b & J \\ J' & J' & 0 \end{pmatrix} \hat{J}'^{-1} \langle a h_1 \mid \chi \mid c h_2 \rangle^0 \langle h_2 b \mid V \mid h_1 d \rangle^0 \quad (59a)$$

$$= (-1)^{2h_1} \hat{J}^{-1} \sum_{J'J''} X \begin{pmatrix} c & d & J \\ a & b & J \\ J' & J' & 0 \end{pmatrix} X \begin{pmatrix} c & a & J' \\ h_2 & h_1 & J' \\ J'' & J'' & 0 \end{pmatrix} \hat{J}''$$

$$\times \langle a h_1 \mid V \mid p_1 p_2 \rangle \langle p_1 p_2 \mid V \mid c h_2 \rangle \langle h_2 b \mid V \mid h_1 d \rangle. \quad (59b)$$

This agrees with the expression given by Barrett and Kirson [9] (diagram 5 of their Appendix) and is probably in a form which is a little more efficient to compute.

Although the vertical cut through the lines h_1 and h_2 in Fig. 16c could easily be

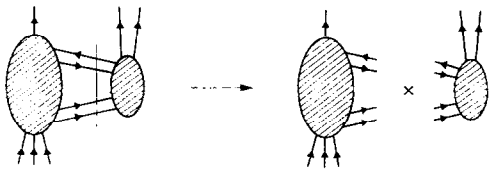

FIG. 15. Factorization by a vertical cut.

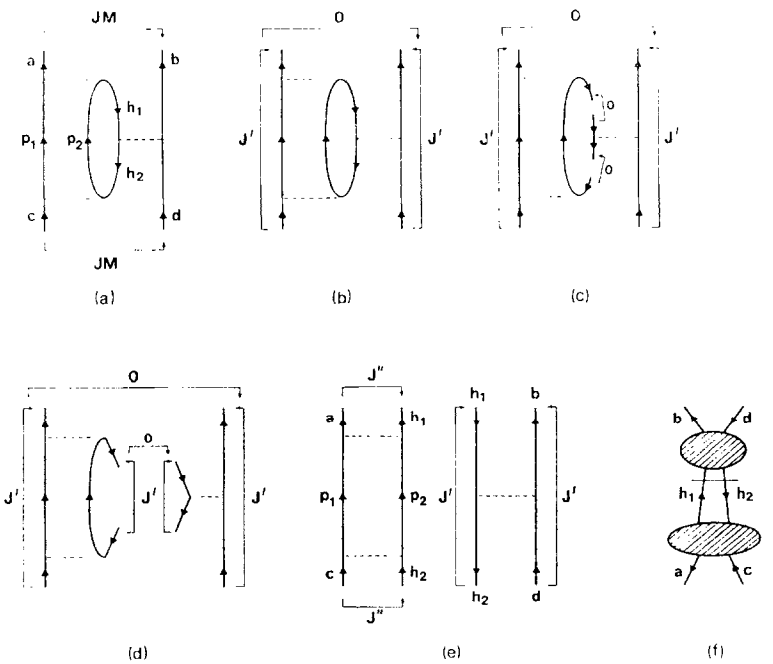

FIG. 16. Decomposition of a complicated diagram into a product of ladders.

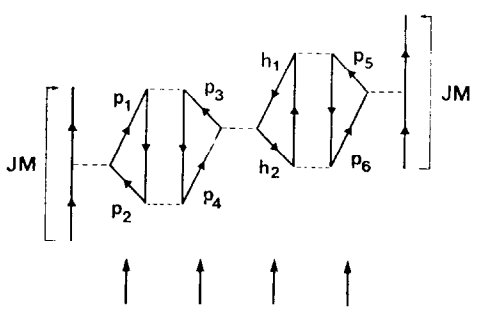

FIG. 17. Generalized particle–hole ladder in the cross channel.

treated as two horizontal cuts, the resulting calculation was somewhat lengthy. This tedious procedure can be circumvented, however, by observing that the diagram is of generalized ladder form when viewed sideways (i.e., in the cross channel). Thus, treating diagram (b) as a generalized particle–hole ladder, as shown in Fig. 16f, we immediately obtain Eq. (59a). In this case the phase $(-1)^{2h_1}$ is due to the phase rule (50), whereas in the former treatment it followed from cutting h_1 and reversing the coupling across the cut. The two approaches are of course equivalent, as the phase rule (50) was originally derived by cutting the internal particle–hole pair in a particle–hole ladder and reversing the coupling across the cut hole line.

To further illustrate the notion of a generalized ladder, we give another example, shown in Fig. 17. Here, the four vertical cuts, indicated by arrows, obviously give a phase factor

$$(-1)^{2p_2+2p_3+2h_1+2p_5}.$$

Note that the cut lines can be either holes or particles.

3.5. *One-Body Insertions*

In the previous subsections we showed that ladder diagrams are particularly simple to evaluate as they factorize into coupled matrix elements of the individual vertices. Also, we showed that more complicated diagrams may be decomposed into products of ladder diagrams by cutting internal lines. Another class of diagrams to which similar simplifications can be applied consists of diagrams with so-called one-body insertions.

A diagram with a one-body insertion has the general structure shown in Fig. 18a. The one-body insertion is denoted by A and may contain any number of V interactions. Since V is a scalar, the line entering and the line leaving A must carry the same j and m

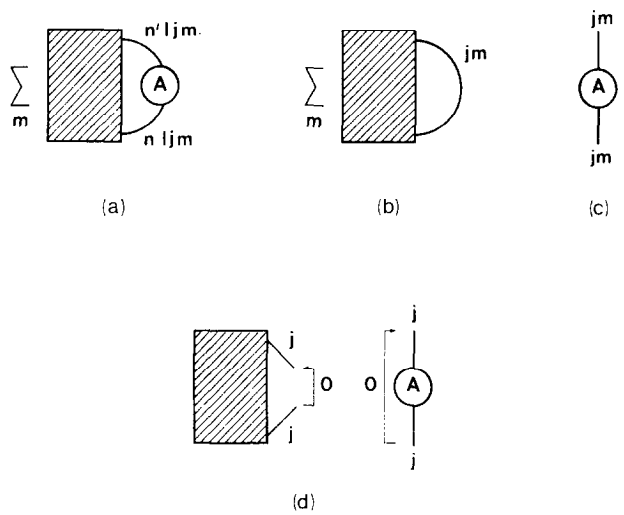

FIG. 18. Factorization of one-body insertions.

quantum numbers. In addition the orbital angular momentum quantum number l must be conserved since V conserves parity. However, the principal quantum numbers n and n' may differ. This should be borne in mind when writing down the complete expression for the diagram, but here we are only interested in the angular momentum properties. In this regard we can write

$$\text{Diagram 18a} = \text{Diagram 18b} \times \text{Diagram 18c}. \tag{60}$$

As indicated in Fig. 18, the z-component m is summed over in diagram 18a, and this summation is carried out in diagram 18b. We emphasize that there is no summation over m in diagram 18c which, of course, is independent of m.

An equivalent result is obtained by cutting off the one-body insertion A by means of a vertical cut, as described in the previous subsection. Since diagram 18a is a scalar coupled particle–hole ladder in the cross channel, it can be written as the product of the two diagrams shown in Fig. 18d, multiplied by the phase $(-1)^{2j}$ deriving from the phase rule (50). Then, by using Eq. (45), the product of Fig. 18d is easily seen to be equivalent to Eq. (60).

Thus we have shown that in determining the angular momentum factors of a diagram, the one-body insertions can be cut off and evaluated separately. Some specific examples will be presented in Section 4 (cases *a*, *b*, *d* and *e*).

3.6. *Effective Operators*

We now discuss the evaluation of diagrams which yield the effective matrix element of an operator T_μ^λ which transforms like a spherical tensor of rank λ, component μ. The operator is defined so that

$$(T_\mu^\lambda)^\dagger = (-1)^{\lambda-\mu} T_{-\mu}^\lambda , \tag{61}$$

consistent with our previous phase convention defined in Subsection 3.1. In a general diagram such as Fig. 19a, the operator T_μ^λ occurs *once* as indicated by the cross. (Note however that the perturbing potential may contain a one-body term U with

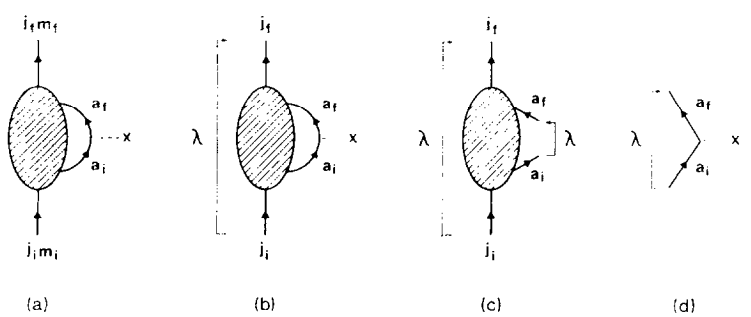

FIG. 19. Decomposition of effective operator diagrams. The operator vertex is denoted by ———×.

$\lambda = 0$, and this can occur *more* than once. This case can also be treated by the methods discussed here.) The blob in Fig. 19a indicates a sequence of V interactions and, of course, the diagram is linked. In Fig. 19a and most of our examples, the valence state consists of a single particle. Our method is general, however, and can be applied to valence states involving arbitrary numbers of particle and hole lines.

By using the Wigner–Eckart theorem we can express the transition matrix elements in terms of *reduced* transition matrix elements which are independent of the magnetic quantum numbers. We shall use the Wigner–Eckart theorem in the following form[5]

$$\langle j_f m_f \mid (V)^m \, T^\lambda_\mu(V)^n \mid j_i m_i \rangle = (-1)^{\lambda-\mu}(-1)^{j_f - m_f} \, C^{j_i \; j_f \; \lambda}_{m_i - m_f - \mu} \langle j_f \| \, (V)^m \, \mathbf{T}^\lambda (V)^n \| \, j_i \rangle, \quad (62)$$

implying that

$$\langle j_f \| \, \mathbf{T}^\lambda \| \, j_i \rangle = (-1)^{\lambda-\mu} \langle j_f \mid T^\lambda_\mu \mid j_i \rangle = \hat{\lambda}^{-1} \langle j_f \mid \mathbf{T}^\lambda \mid j_i \rangle^0, \quad (63)$$

where the last matrix element is explicitly coupled to a resultant angular momentum of zero, as indicated by the superscript. Note also that by using Eq. (61) we obtain

$$\langle j_2 \| \, \mathbf{T}^\lambda \| \, j_1 \rangle = (-1)^{j_2 + \lambda - j_1} \langle j_1 \| \, \mathbf{T}^\lambda \| \, j_2 \rangle, \quad (64)$$

where we have taken the reduced matrix element to be real, as will always be the case here.

It is the reduced matrix element which we shall define to be the value of a given diagram and which we shall evaluate. To be more explicit, we define the value of the diagram in Fig. 19a to be that of Fig. 19b where the external lines i and f are coupled. Clearly, the diagram in Fig. 19b is just the reduced matrix element defined in Eq. (63). On the other hand, if we wish to compute the m-scheme matrix element corresponding to Fig. 19a, we can simply use Eq. (62). Note that if we are dealing with hole rather than particle states, we should use Eq. (63) with the labels i and f interchanged.

Now, to calculate the reduced matrix element of Fig. 19b, we notice that it has the form of a particle–hole ladder in the cross channel. Thus, we can use the techniques of the previous subsections to express it as the product of the two diagrams shown in Figs. 19c and d, multiplied by a phase $(-1)^{2a_f}$ coming from the phase rule (50). Firstly, by definition diagram (d) gives a contribution

$$\text{Diagram 19d} = \langle a_f \| \, \mathbf{T}^\lambda \| \, a_i \rangle. \quad (65)$$

Secondly, in diagram (c) we have coupled $j_i(a_i)$ and $j_f(a_f)$ to a resultant angular momentum λ, so that the diagram is in the cross-coupled form already discussed for the effective interaction. It is independent of μ, the z-component of λ, so that, if desired, we can further couple the two angular momenta λ to a resultant angular momentum of zero, provided that a factor $\hat{\lambda}^{-1}$ is introduced. This is sometimes convenient, as we shall see.

[5] The reduced matrix element defined here is $(-1)^{j_i+\lambda-j_f} \, \hat{\lambda}^{-1}$ times that of Edmonds [18].

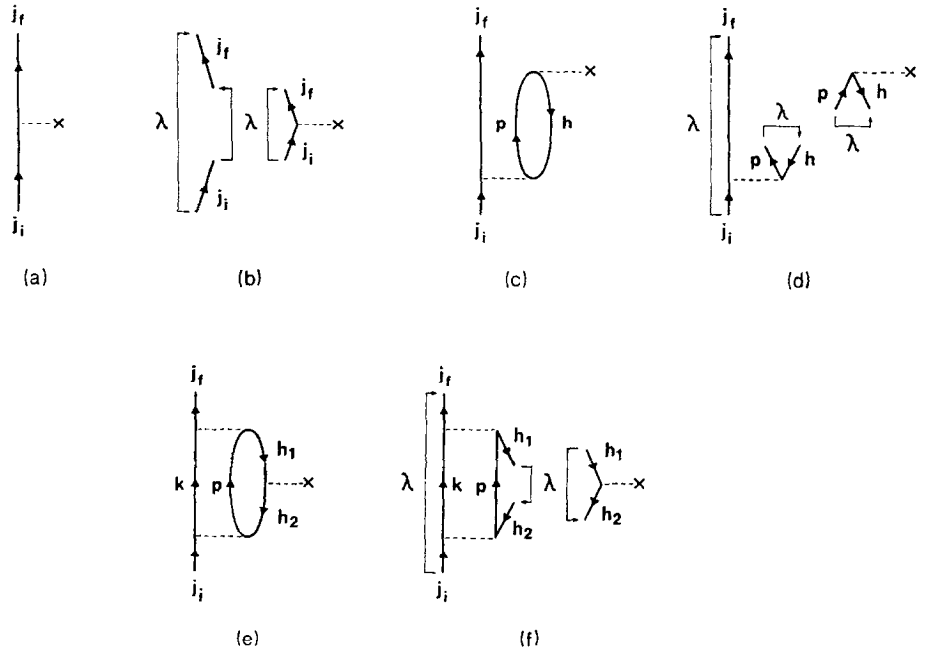

FIG. 20. Some low-order effective operator diagrams.

Our rule for obtaining the value of an effective operator diagram like Fig. 19b (i.e., the reduced matrix element) is therefore to write it as a product

$$\text{Diagram 19b} = (-1)^{2a_f} \times \text{Diagram 19c} \times \text{Diagram 19d}, \tag{66}$$

where diagram 19c can be evaluated by the techniques discussed previously and diagram 19d is given by Eq. (65).

Let us give a few examples. The most simple diagram is given in Fig. 20a, and this is pulled apart in Fig. 20b. Since we have two Clebsch–Gordan coefficients coupling j_i and j_f to λ, the sum over z-components gives unity. In addition there is a phase $(-1)^{2j_f}$ which cancels the phase $(-1)^{2a_f}$ in Eq. (66), and so we obtain the obvious result

$$\text{Diagram 20a} = \langle j_f \| \mathbf{T}^\lambda \| j_i \rangle. \tag{67}$$

The diagram of Fig. 20c is evaluated in the form indicated in Fig. 20d, giving

$$\text{Diagram 20c} = (-1)^{2h} \langle j_f p \mid V \mid j_i h \rangle \langle h \| \mathbf{T}^\lambda \| p \rangle, \tag{68}$$

where as usual the phases and factors associated with the corresponding uncoupled

diagram have been left out. As a final example consider Fig. 20e, which is evaluated in the form of Fig. 20f:

$$\text{Diagram 20e} = (-1)^{2h_2}\langle j_f h_1 \mid \chi \mid j_i h_2\rangle\langle h_2 \| \mathbf{T}^\lambda \| h_1\rangle$$

$$= (-1)^{2h_2}(-1)^{h_1+h_2-\lambda}\hat{\lambda}^{-1}\sum_J X\begin{pmatrix} j_i & j_f & \lambda \\ h_2 & h_1 & \lambda \\ J & J & 0 \end{pmatrix}\hat{J}$$

$$\times \langle j_f h_1 \mid V \mid kp\rangle\langle kp \mid V \mid j_i h_2\rangle\langle h_2 \| \mathbf{T}^\lambda \| h_1\rangle. \tag{69}$$

Note the similarity here to the evaluation of Fig. 16a in Subsection 3.4. The above expressions agree with those given by Siegel and Zamick [15].

The present technique may be generalized to treat more complicated cases, such as the two-body effective operator diagrams. Consider as an example the diagram of Fig. 21a. We first cut off the operator vertex, and write the diagram as the product of Figs. 21b and c, multiplied by a phase deriving from the phase rule (50). The techniques described in Subsections 3.1 to 3.5 can be readily used to evaluate Fig. 21b.

3.7. *Further Remarks*

Our basic approach has been to break a given diagram into a product of ladder diagrams which are easily dealt with. Up to now, we have not considered cases with three or more valence lines. We shall now discuss the angular momentum factors associated with such diagrams. An example of an effective interaction diagram with three valence lines is shown in Fig. 22a. Such a diagram contributes to the effective interaction for nuclei with three nucleons outside closed shells, for instance ^{19}O. The diagram of Fig. 22a does not appear to have an obvious ladder form. It is composed of five ladders, but each has only one rung, i.e., one interaction vertex. The diagram of Fig. 22b has in fact the same basic structure, although it only has two valence lines. This is seen by cutting and pulling open the hole line. This type of diagram is usually called a three-body cluster.

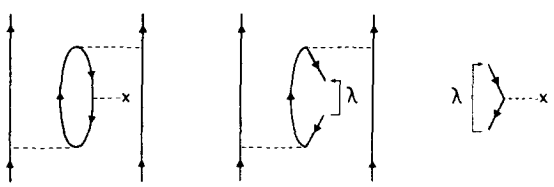

FIG. 21. Treatment of a two-body effective operator diagram.

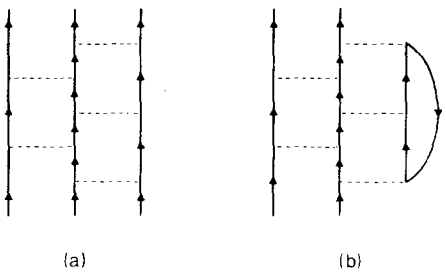

FIG. 22. Three-body cluster diagram.

The basic principle for determining the angular momentum structure of such diagrams remains the same, namely we break the diagrams into products of ladders (including those with one rung). By systematically recoupling and successively breaking off ladders, the procedure is indeed straightforward. This is clearly illustrated by the example shown in Fig. 23. It is readily seen that the lower two-body ladder can be broken off yielding

$$\text{Diagram 23a} = \sum_{J_{23}} X \begin{pmatrix} j_1 & j_2 & J_{12} \\ 0 & j_3 & j_3 \\ j_1 & J_{23} & J \end{pmatrix} \times \text{Diagram 23b} \times \text{Diagram 23c}, \qquad (70)$$

with the obvious restriction $J_{23} = J_{45}$. Clearly, the basic building blocks, such as diagrams (b) and (c) in this example, may appear in several diagrams, but they only need to be evaluated once. This procedure may be generalized in a straightforward manner to treat diagrams with more than three valence lines, such as the four-body clusters.

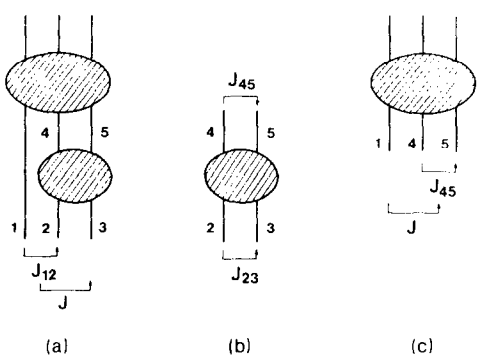

FIG. 23. Factorization of a three-body diagram.

4. Summary and Illustrative Examples

In this section we work out some examples which illustrate the power of the present technique. It is useful first to summarize the basic steps of our procedure:

(i) In the first step we use the diagram rules for the uncoupled representation, as discussed in Section 2, to obtain all factors aside from angular momentum coupling.

(ii) Then, the angular momentum factors are obtained by the following procedure:

(a) First, it is often convenient to couple the diagram explicitly to a scalar.

(b) Then, the diagram is decomposed into products of ladder diagrams, insofar as is possible, by angular momentum recoupling, by cutting internal lines, etc., as explained in Section 3. Since in general there are many different ways of cutting a diagram, we have not given explicit rules for the angular momentum factors and phases associated with a given cut, except for the simple cases shown in Fig. 14 and the phase rule (50) which applies to cuts of particle–hole pairs where the lines are coupled in the same order on each side of the cut. However, for all other cuts the angular momentum factors and phases can easily be worked out using standard angular momentum algebra.

(c) Each ladder is readily expressed in terms of standard coupled and cross-coupled matrix elements, keeping in mind rule (e), below.

(d) One-body insertions can be cut off and treated separately.

(e) There are special phase factors associated with particle–hole pairs, namely,

$$(-1)^{n_{tph}+n_{ph}}, \tag{71}$$

where n_{tph} is the number of particle–hole pairs on the top (bra) side of the diagram and n_{ph} is the number of internal particle–hole pairs cut open for which the particle and hole lines are coupled in the same direction across the cut. Recall that the second part of this phase rule $[(-1^{n_{ph}}]$ is operational in the sense that it may give different phases for different decompositions of a given diagram. Any such phase difference will of course be compensated by other phase differences in the components of the diagram. The phase (71) arises from angular momentum considerations alone. Thus, if isospin couplings are considered as well, this phase arises twice and can therefore be ignored.

(f) Finally, we sum over all intermediate-state quantum numbers.

We now use this technique to calculate the diagrams of Fig. 3; the slashes on these diagrams are to indicate where we have cut the lines. For each case, we briefly outline the steps that are needed to arrive at a given formula. We give the results in terms of the X-coefficients since this is most transparent, however the expressions can be simplified by using Eqs. (30)–(32). For simplicity we do not explicitly indicate the summation over intermediate particle and hole states. Further, only j out of the set of labels nlj

needed to specify a single-particle state is indicated in the matrix elements. (Note that if j_1 is required to be equal to j_2, this does not imply $n_1 = n_2$.)

We shall give both the angular momentum and the isospin factors; the latter are obtained from the former by replacing the single-particle angular momenta j by $\frac{1}{2}$ and substituting T labels for J labels. Thus the standard JT coupled matrix elements which we shall use are obtained by making these substitutions in Eq. (17), while the cross-coupled matrix elements are defined by Eq. (43). We also show explicitly the phase factor (71) even though it is the same for angular momentum and isospin and therefore contributes $+1$. Further, the normalization factors for external lines will be included. They are needed when the external lines are coupled to total angular momentum J and isospin T. For example, for the diagram of Fig. 3f we need an extra factor of $[(1 + \delta_{j_a j_b})(1 + \delta_{j_c j_d})]^{-1/2}$. We should point out that our standard coupled matrix elements of Eq. (17) do *not* include these factors. Thus, they are related to the usual two-particle matrix elements, say those of Kuo and Brown [16], by

$$\overset{JT}{\langle}ab \mid V \mid cd\overset{JT}{\rangle} = \sqrt{(1 + \delta_{ab})(1 + \delta_{cd})}\,\langle abJT \mid V_{\mathbf{KB}} \mid cdJT\rangle. \tag{72}$$

This applies to all of the examples given in this section. In Eq. (72) and throughout this section we have replaced $JMTM_T$ by the less cumbersome JT despite the fact that none of the matrix elements are scalar coupled.

Expressions for several of the diagrams considered here can be found in the works of Kassis [17], Barrett and Kirson [9] and Siegel and Zamick [15]. In many cases, our expressions appear to be somewhat more transparent in structure and efficient for computation.

EXAMPLE a. Cutting Fig. 3a as indicated, we couple the h_4 lines to a scalar and similarly for the p_2 lines, obtaining a factor $\hat{h}_4\hat{\tfrac{1}{2}}\hat{p}_2\hat{\tfrac{1}{2}}$. Coupling also p_1 and h_3 (necessarily to a scalar) we can recouple to obtain

$$\begin{aligned}
\text{Diagram 3a} = &-\tfrac{1}{2}[(\epsilon_{h_3} - \epsilon_{p_1})(\epsilon_{h_1} + \epsilon_{h_2} - \epsilon_{p_1} - \epsilon_{p_2})]^{-1} \sum_{\substack{JT\\J'T'}} (-1)^{2(h_3+1/2)}(-1)^{2(h_3+1/2)} \\
&\times \hat{h}_4\hat{\tfrac{1}{2}}\hat{p}_2\hat{\tfrac{1}{2}}\hat{J}\hat{T}\hat{J}'\hat{T}' X\begin{pmatrix} p_1 & h_3 & 0 \\ h_4 & h_4 & 0 \\ J & J & 0 \end{pmatrix} X\begin{pmatrix} \frac{1}{2} & \frac{1}{2} & 0 \\ \frac{1}{2} & \frac{1}{2} & 0 \\ T & T & 0 \end{pmatrix} X\begin{pmatrix} h_3 & p_1 & 0 \\ p_2 & p_2 & 0 \\ J' & J' & 0 \end{pmatrix} X\begin{pmatrix} \frac{1}{2} & \frac{1}{2} & 0 \\ \frac{1}{2} & \frac{1}{2} & 0 \\ T' & T' & 0 \end{pmatrix} \\
&\times \overset{JT}{\langle}h_3h_4 \mid V \mid p_1h_4\overset{JT}{\rangle}\overset{J'T'}{\langle}h_1h_2 \mid V \mid h_3p_2\overset{J'T'}{\rangle}\overset{J'T'}{\langle}p_1p_2 \mid V \mid h_1h_2\overset{J'T'}{\rangle} \\
= &-\tfrac{1}{2}[(\epsilon_{h_3} - \epsilon_{p_1})(\epsilon_{h_1} + \epsilon_{h_2} - \epsilon_{p_1} - \epsilon_{p_2})]^{-1} \sum_{\substack{JT\\J'T'}} (-1)^{2(h_3+1/2)}(-1)^{2(h_3+1/2)} \\
&\times [\hat{p}_1\hat{\tfrac{1}{2}}]^{-2}[\hat{J}\hat{T}\hat{J}'\hat{T}']^2\overset{JT}{\langle}h_3h_4 \mid V \mid p_1h_4\overset{JT}{\rangle}\overset{J'T'}{\langle}h_1h_2 \mid V \mid h_3p_2\overset{J'T'}{\rangle}\overset{J'T'}{\langle}p_1p_2 \mid V \mid h_1h_2\overset{J'T'}{\rangle}.
\end{aligned} \tag{73}$$

Here and in the following we have collected the phases and factors associated with the diagram in uncoupled form in front of the summation sign. Apart from the energy denominators these can be inferred from Table I. Recall also that the entire expression has to be summed over the intermediate particle and hole states. In Eq. (73) one of the phase factors $(-1)^{2(h_3+1/2)}$ comes from cutting the particle–hole pair p_1h_3, while the other comes from inverting the scalar coupling between p_1 and h_3 in the lower part of the diagram.

EXAMPLE b. We first cut off the one-body insertion of Fig. 3b using the technique of Fig. 18d. The remaining diagram is in the form of a ladder if we cut open the h_1 line. Noting that $h_2 = h_3$, we have

$$\text{Diagram 3b} = -\frac{1}{2^2}[(\epsilon_{h_1}+\epsilon_{h_2}-\epsilon_{p_3}-\epsilon_{p_4})(\epsilon_{h_1}+\epsilon_{h_2}-\epsilon_{p_1}-\epsilon_{p_2})$$

$$\times(\epsilon_{h_1}+\epsilon_{h_3}-\epsilon_{p_1}-\epsilon_{p_2})]^{-1}\sum_{\substack{JT\\J'T'}}(-1)^{2(h_2+1/2)}(-1)^{2(h_2+1/2)}[\hat{h}_2\hat{\hat{1}}]^{-2}$$

$$\times[\hat{J}\hat{T}\hat{J}'\hat{T}']^2\langle h_1h_2 \mid V \mid p_3p_4\rangle_{JT}\langle p_3p_4 \mid V \mid p_1p_2\rangle_{JT}\langle p_1p_2 \mid V \mid h_1h_3\rangle_{JT}$$

$$\times\langle h_3h_4 \mid V \mid h_2h_4\rangle_{J'T'}. \tag{74}$$

Here, a phase $(-1)^{2(h_2+1/2)}$ is obtained by cutting off the one-body insertion, since this amounts to cutting a particle–hole ladder in the cross channel. Further, another phase $(-1)^{2(h_2+1/2)}$ is obtained by inverting the scalar coupling between h_2 and h_3 in the one-body insertion so that the proper "in" coupled to "out" ordering is obtained.

EXAMPLE c. We cut open the h_1 line of Fig. 3c and couple the pieces to a scalar. Since we must have $a = c$, we also couple the complete diagram to a scalar. This allows us to recouple the diagram to ladder form, obtaining

$$\text{Diagram 3c} = +\frac{1}{2^2}[(\epsilon_c+\epsilon_{h_1}-\epsilon_{p_1}-\epsilon_{p_2})(\epsilon_{h_3}+\epsilon_{h_2}-\epsilon_{p_1}-\epsilon_{p_2})]^{-1}$$

$$\times\sum_{JT}[\hat{c}\hat{\hat{1}}]^{-2}[\hat{J}\hat{T}]^2\langle ah_1 \mid V \mid p_1p_2\rangle_{JT}\langle h_3h_2 \mid V \mid ch_1\rangle_{JT}\langle p_1p_2 \mid V \mid h_3h_2\rangle_{JT}. \tag{75}$$

EXAMPLE d. We cut off the one-body insertion. The remaining diagram is already in ladder form and noting that $a = c$ and $p_1 = p_2$, we have

$$\text{Diagram 3d} = -\tfrac{1}{2}[(\epsilon_{h_1} + \epsilon_{h_2} - \epsilon_a - \epsilon_{p_1})(\epsilon_{h_1} + \epsilon_{h_2} - \epsilon_a - \epsilon_{p_2})]^{-1}$$

$$\times \sum_{\substack{JT \\ J'T'}} (-1)^{2(p_1+1/2)}(-1)^{2(p_1+1/2)}[\hat{c}\hat{\tfrac{1}{2}}\hat{p}_1\hat{\tfrac{1}{2}}]^{-2}[\hat{J}\hat{T}\hat{J}'\hat{T}']^2$$

$$\times \langle h_1h_2 \mid V \mid cp_1\rangle\langle ap_2 \mid V \mid h_1h_2\rangle\langle p_1h_3 \mid V \mid p_2h_3\rangle. \tag{76}$$

The two phases inside the summation have similar origin to example (b).

EXAMPLE e. We cut the line labelled p_2 in Fig. 3e and note that $p_2 = d$. The one-body part can then be treated as in Fig. 12 so we find

$$\text{Diagram 3e} = -\tfrac{1}{2}[(\epsilon_c + \epsilon_b + \epsilon_{h_1} + \epsilon_{h_2} - \epsilon_d - \epsilon_a - \epsilon_{p_2} - \epsilon_{p_1})$$

$$\times (\epsilon_{h_1} + \epsilon_{h_2} - \epsilon_d - \epsilon_{p_1})]^{-1} \sum_{J'T'} (-1)^{2(b+1/2)}(-1)^{2(p_2+1/2)}(-1)^{2(p_2+1/2)}$$

$$\times [\hat{d}\hat{\tfrac{1}{2}}]^{-2}[\hat{J}'\hat{T}']^2\langle ap_2 \mid V \mid bc\rangle\langle h_1h_2 \mid V \mid p_2p_1\rangle\langle dp_1 \mid V \mid h_1h_2\rangle. \tag{77}$$

Here, the phase $(-1)^{2(b+1/2)}$ comes from the phase rule (71) [or (40)] as there is one particle–hole pair on the top side of the diagram. Then, we obtain a phase $(-1)^{2(p_2+1/2)}$ by inverting the scalar coupling of the two pieces of the p_2 line at the cut and another phase $(-1)^{2(p_2+1/2)}$ by inverting the scalar coupling of p_2 and d obtained by angular momentum recoupling.

EXAMPLE f. We cross-couple the external legs of Fig. 3f and cut the p_1h_1 pair to obtain the product of two ladder diagrams. Care should be taken to keep track of the phases arising from changes in the coupling order. After performing the appropriate recouplings we obtain

$$\text{Diagram 3f} = +[(1 + \delta_{ab})(1 + \delta_{cd})]^{-1/2}[(\epsilon_c + \epsilon_{h_1} - \epsilon_{p_1} - \epsilon_b)$$

$$\times (\epsilon_c + \epsilon_{h_2} - \epsilon_{p_1} - \epsilon_{p_2})]^{-1} \sum_{\substack{J'T' \\ J''T''}} (-1)^{2(h_1+1/2)}(-1)^{2(h_2+1/2)}(-1)^{c+d-J+1-T}$$

$$\times [\hat{J}\hat{T}]^{-1}\hat{J}''\hat{T}''X\begin{pmatrix} d & c & J \\ a & b & J \\ J' & J' & 0 \end{pmatrix} X\begin{pmatrix} \frac{1}{2} & \frac{1}{2} & T \\ \frac{1}{2} & \frac{1}{2} & T \\ T' & T' & 0 \end{pmatrix}\langle ah_1 \mid V \mid dp_1\rangle$$

$$\times X\begin{pmatrix} c & b & J' \\ p_1 & h_1 & J' \\ J'' & J'' & 0 \end{pmatrix} X\begin{pmatrix} \frac{1}{2} & \frac{1}{2} & T' \\ \frac{1}{2} & \frac{1}{2} & T' \\ T'' & T'' & 0 \end{pmatrix}\langle h_2b \mid V \mid h_1p_2\rangle\langle p_1p_2 \mid V \mid h_2c\rangle. \tag{78}$$

Here, the phase $(-1)^{c+d-J+1-T}$ obviously comes from inverting the coupling between the external lines c and d. Further, the phase $(-1)^{2(h_1+1/2)}$ is obtained by cutting the particle–hole pair p_1h_1, while the phase $(-1)^{2(h_2+1/2)}$ is due to the factorization of the remaining particle–hole ladder with intermediate state p_2h_2.

EXAMPLE g. We cross-couple the external legs of Fig. 3g and cut the p_1h_1 pair. The right-hand part of the diagram is tackled by cutting the p_2p_4 pair so as to give a one-rung ladder and a core-polarization diagram whose evaluation was discussed in Subsection 3.3. Explicitly we find

$$\begin{aligned}\text{Diagram 3g} = &+[(1+\delta_{ab})(1+\delta_{cd})]^{-1/2}[(\epsilon_c+\epsilon_d+\epsilon_{h_1}-\epsilon_a-\epsilon_{p_2}-\epsilon_{p_4})\\
&\times(\epsilon_c+\epsilon_{h_1}+\epsilon_{h_2}-\epsilon_a-\epsilon_{p_2}-\epsilon_{p_3})(\epsilon_c+\epsilon_{h_1}-\epsilon_a-\epsilon_{p_1})]^{-1}\\
&\times\sum_{\substack{J_1T_1\\J_2T_2\\J_3T_3}}(-1)^{2(h_1+1/2)}(-1)^{2(h_2+1/2)}[\hat{J}\hat{T}]^{-1}\,\hat{J}_3\hat{T}_3X\begin{pmatrix}c&d&J\\a&b&J\\J_1&J_1&0\end{pmatrix}X\begin{pmatrix}\frac12&\frac12&T\\\frac12&\frac12&T\\T_1&T_1&0\end{pmatrix}\\
&\times X\begin{pmatrix}p_1&h_1&J_1\\d&b&J_2\\J_2&J_2&0\end{pmatrix}X\begin{pmatrix}\frac12&\frac12&T_1\\\frac12&\frac12&T_1\\T_2&T_2&0\end{pmatrix}X\begin{pmatrix}p_1&d&J_2\\p_2&p_4&J_2\\J_3&J_3&0\end{pmatrix}X\begin{pmatrix}\frac12&\frac12&T_2\\\frac12&\frac12&T_2\\T_3&T_3&0\end{pmatrix}\\
&\times\langle h_1b\mid V\mid p_2p_4\rangle\langle h_2p_4\mid V\mid p_3d\rangle\langle p_2p_3\mid V\mid p_1h_2\rangle\langle ap_1\mid V\mid ch_1\rangle.\end{aligned}\tag{79}$$

Here, the phase $(-1)^{2(h_1+1/2)}$ comes from cutting the particle–hole pair p_1h_1, whereas the phase $(-1)^{2(h_2+1/2)}$ arises from factorization of the core-polarization "ladder" with intermediate state p_3h_2. The derivation of the above expression would probably become much more difficult without the present technique.

EXAMPLE h. The diagram of Fig. 3h is in ladder form already, provided that we cross-couple the external legs. We find

$$\begin{aligned}\text{Diagram 3h} = &+\tfrac12(1+\delta_{ab})^{-1/2}(\epsilon_c+\epsilon_d-\epsilon_{p_1}-\epsilon_{p_2})^{-1}\\
&\times(-1)^{2(d+1/2)}[\hat{c}\hat{\tfrac12}]^{-1}\,\hat{J}\hat{T}X\begin{pmatrix}0&c&c\\J&d&c\\J&J&0\end{pmatrix}X\begin{pmatrix}0&\frac12&\frac12\\T&\frac12&\frac12\\T&T&0\end{pmatrix}\\
&\times\langle ab\mid V\mid p_1p_2\rangle\langle p_1p_2\mid V\mid cd\rangle.\end{aligned}\tag{80}$$

Here, the phase $(-1)^{2(d+1/2)}$ arises from the top particle–hole pair.

EXAMPLE i. We take our tensor operator to be the product of an operator T_u^{λ} acting in ordinary space and an operator T_v^{τ} acting in isospin space. Cutting off the operator in Fig. 3i as shown in Fig. 19 and recoupling to obtain a ladder, we find for the reduced matrix element (in both ordinary and isospin space)

$$\begin{aligned}\text{Diagram 3i} = &+[(\epsilon_a + \epsilon_{h_1} - \epsilon_{p_2} - \epsilon_{p_3})(\epsilon_c + \epsilon_{h_1} - \epsilon_{p_1} - \epsilon_{p_3})]^{-1} \\ &\times \sum_{JT} (-1)^{2(p_2+1/2)}(-1)^{2(h_1+1/2)} \langle p_2 \| \mathbf{T}^{\lambda} \| p_1 \rangle \langle \tfrac{1}{2} \| \mathbf{T}^{\tau} \| \tfrac{1}{2} \rangle [\hat{\lambda}\hat{\tau}]^{-1} \hat{J}\hat{T} \\ &\times X \begin{pmatrix} c & a & \lambda \\ p_1 & p_2 & \lambda \\ J & J & 0 \end{pmatrix} X \begin{pmatrix} \frac{1}{2} & \frac{1}{2} & \tau \\ \frac{1}{2} & \frac{1}{2} & \tau \\ T & T & 0 \end{pmatrix} \langle ah_1 \mid V \mid p_3 p_2 \rangle \langle p_3 p_1 \mid V \mid ch_1 \rangle .\end{aligned} \tag{81}$$

Here, the phase $(-1)^{2(p_2+1/2)}$ is obtained by cutting off the one-body operator, since this amounts to cutting a particle–hole pair in the cross channel. Further, there is a phase $(-1)^{2(h_1+1/2)}$ coming from the factorization of the remaining ladder diagram with the particle–hole intermediate state $p_3 h_1$.

EXAMPLE j. The diagram of Fig. 3j is an example of a two-body effective operator diagram. By cutting off the operator and recoupling twice, we can express the diagram as the product of a two-body ladder diagram and a simple one-body operator diagram, obtaining

$$\begin{aligned}\text{Diagram 3j} = &+\tfrac{1}{2}[(\epsilon_c + \epsilon_d - \epsilon_{p_2} - \epsilon_{p_3})(\epsilon_d - \epsilon_{p_1})]^{-1} \langle p_1 \| \mathbf{T}^{\lambda} \| d \rangle \langle \tfrac{1}{2} \| \mathbf{T}^{\tau} \| \tfrac{1}{2} \rangle \\ &\times \hat{p}_1 \hat{\tfrac{1}{2}} \hat{J}_f \hat{T}_f X \begin{pmatrix} c & d & J_i \\ p_1 & p_1 & 0 \\ J_f & \lambda & J_i \end{pmatrix} X \begin{pmatrix} \frac{1}{2} & \frac{1}{2} & T_i \\ \frac{1}{2} & \frac{1}{2} & 0 \\ T_f & \tau & T_i \end{pmatrix} X \begin{pmatrix} J_f & \lambda & J_i \\ J_f & 0 & J_f \\ 0 & \lambda & \lambda \end{pmatrix} X \begin{pmatrix} T_f & \tau & T_i \\ T_f & 0 & T_f \\ 0 & \tau & \tau \end{pmatrix} \\ &\times \langle ab \mid V \mid p_2 p_3 \rangle \langle p_2 p_3 \mid V \mid cp_1 \rangle .\end{aligned} \tag{82}$$

ACKNOWLEDGMENT

One of the authors (T.T.S.K.) would like to thank Professor A. Faessler for many helpful discussions and his hospitality at Jülich.

REFERENCES

1. T. T. S. KUO, S. Y. LEE, AND K. F. RATCLIFF, *Nucl. Phys. A* **176** (1971), 65.
2. T. T. S. KUO, *Ann. Rev. Nucl. Sci.* **24** (1974), 101.
3. B. H. BRANDOW, *Rev. Mod. Phys.* **39** (1967), 771.

4. P. J. ELLIS AND E. OSNES, *Rev. Mod. Phys.* **49** (1977), 777.
5. J. SHURPIN, D. STROTTMAN, T. T. S. KUO, M. CONZE, AND P. MANAKOS, *Phys. Lett. B* **69** (1977), 395.
6. J. SHURPIN, H. MÜTHER, T. T. S. KUO, AND A. FAESSLER, *Nucl. Phys. A* **293** (1977), 61.
7. E. M. KRENCIGLOWA AND T. T. S. KUO, *Nucl. Phys. A* **240** (1975), 195.
8. P. J. ELLIS, *in* "Proceedings of the International Topical Conference on Effective Interactions and Operators in Nuclei," Tuscon, 1975 (B. R. Barrett, Ed.), Lecture Notes in Physics No. 40, p. 296, Springer-Verlag, Berlin, 1975.
9. B. R. BARRETT AND M. W. KIRSON, *Nucl. Phys. A* **148** (1970), 145.
10. P. GOODE AND D. S. KOLTUN, *Nucl. Phys. A* **243** (1975), 44.
11. N. M. HUGENHOLTZ, *Physica* **23** (1957), 481.
12. T. T. S. KUO AND E. OSNES, "Many-Body Theory for Nuclear Structure," monograph in preparation.
13. M. BARANGER, *Phys. Rev.* **120** (1960), 957.
14. E. OSNES, T. T. S. KUO, AND C. S. WARKE, *Nucl. Phys. A* **168** (1971), 190.
15. S. SIEGEL AND L. ZAMICK, *Nucl. Phys. A* **145** (1970), 89.
16. T. T. S. KUO AND G. E. BROWN, *Nucl. Phys.* **85** (1966), 40.
17. N. I. KASSIS, *Nucl. Phys. A* **194** (1972), 205.
18. A. R. EDMONDS, "Angular Momentum in Quantum Mechanics," p. 75, Princeton Univ. Press, Princeton, N.J., 1957.
19. G. F. BERTSCH, "The Practitioner's Shell Model," p. 147, American Elsevier, New York, 1972.